Mathematical Modeling of Lithium Batteries

Karen E. Thomas and Robert M. Darling and John Newman

13th December 2021

1 Previous Reviews

Previous reviews of the equations, numerical methods, and uses of models of lithium batteries are given in references [1, 2, 3, 4]. We refer the reader to these reviews for references regarding early works, and focus in this paper on work published since these reviews. However, we acknowledge that much of the theory used in modeling lithium batteries was developed previously for other battery systems, such as lead acid, alkaline zinc-MnO_2, molten salt LiAl-FeS, and nickel-metal hydride. When citing the development of some model formulations, we cite these original works even though they do not specifically apply to lithium batteries.

Early work on modeling lithium batteries, performed prior to the ready availability of high-speed digital computers, used simplified models neglecting kinetic or concentration effects, assuming constant properties, or neglecting the separator, in order to obtain a close approximation to battery behavior within the limits of computational power available at the time. Today's computers can easily simulate the entire cell sandwich, obviating the need for the simplifying assumptions used previously. We therefore see no need to review the history of the development of the full-cell-sandwich model, and simply present the model in the best form developed to date in section 3, followed by considerations of special situations which are not essential to the basic modeling framework. Simplifying cases which have contributed to our understanding of the lithium battery are presented in section 5. Finally, we discuss applications of modeling, such as interpreting experimental data and optimizing geometric parameters.

2 Features of the lithium battery

Figure 1 shows a schematic of a lithium battery. Lithium battery electrodes are usually made by coating a slurry of the active material, conductive filler, and binder onto a foil current collector. This porous configuration provides a high surface area for reaction and reduces the distance between reactants and the surfaces where reactions occur. In these

porous electrodes, the electrochemical reaction is distributed over the surface of the particles of active material, and will vary across the depth of the electrode due to the interaction of potential drop and concentration changes in both the solution and solid phases. Porous electrode theory is used to understand these interactions.

Most electrodes used in lithium batteries are insertion compounds. In an insertion reaction, lithium ions from solution combine with an electron in the electrode to reside in an interstitial site in the host lattice. Such materials exhibit long cycle lives because the electrochemical reaction causes relatively little disturbance to the active material. They are also rather convenient to model, because volume changes can usually be neglected, and there is little change in the morphology of the electrode during cycling. In contrast to phase-change electrodes, such as the $Cd|Cd(OH)_2$ electrode, the potential of the solid material in insertion electrodes varies with state of charge (*i.e.*, lithium concentration). The combination of lithium diffusion in the solid phase and the nonlinear dependence of the chemical potential on lithium concentration lead to interesting situations in these materials.

The organic electrolytes used in lithium batteries generally exhibit nonideal behavior, and usually concentrated solutions of 1 to 1.5 M are used. Moreover, mass transport in the nonaqueous electrolytes used in lithium batteries often has a large impact on battery performance at moderate to high current densities, and cannot be assumed to be negligible. Fortunately, the electrolyte in most cases consists of a single salt in a homogeneous solvent, a case which is easily treated rigorously by concentrated solution theory. The solvent may be a single liquid, a mixture of liquids, a gel, or a polymer. Technically in solvent mixtures, ions will interact differently with the different solvent components, causing gradients in solvent composition as ions drag solvent molecules along with them during passage of current. However, for realistic battery electrolyte conditions, the assumption that a solvent mixture behaves as a single solvent does not appear to introduce significant error[5]. Electrolytes with multiple salts and solvents can be treated using concentrated solution theory[6, 7, 8], although experimental determination of the complete set of transport properties is difficult. For an electrolyte of n ions and solvent species, $n(n-1)/2$ transport properties are required to describe mass transport completely.

A battery consists of three regions: positive electrode, negative electrode, and separator. The importance of considering interactions among mass transport and potential in the electrolyte in all three regions when considering solution-phase limitations in one of the regions has been demonstrated[9].

3 Basic equations

In this section we describe the equations required to simulate the electrochemical performance of porous electrodes with concentrated electrolytes. Extensions to this basic model are presented in section 4. The basis of porous electrode theory and concentrated solution

theory has been reviewed by Newman and Tiedemann[1]. In porous electrode theory, the exact positions and shapes of all the particles and pores in the electrode are not specified. Instead, properties are averaged over a volume small with respect to the overall dimensions of the electrode but large with respect to the pore structure. The electrode is viewed as a superposition of active material, filler, and electrolyte, and these phases coexist at every point in the model. Particles of the active material generally can be treated as spheres. The electrode phase is coupled to the electrolyte phase via mass balances and via the reaction rate, which depends on the potential difference between the phases. All phases are considered to be electrically neutral, which assumes that the volume of the double layer is small relative to the pore volume. Where applicable, we also indicate boundary conditions that would be used if a lithium foil electrode were used in place of a negative insertion electrode.

3.1 Potential in the electrolyte

We define the potential in the binary electrolyte to be measured by a reference electrode that undergoes the reversible half-cell reaction

$$s_- M_-^{z_-} + s_+ M_+^{z_+} + s_o M_o \rightleftharpoons n e^- \tag{1}$$

The gradient of the potential in the solution, as measured by such a reference electrode with respect to another reference electrode of the same kind at a fixed position, is then determined by[10]

$$\nabla \Phi_2 = -\frac{i_2}{\kappa} - \frac{\nu RT}{F} \left(\frac{s_+}{n\nu_+} + \frac{t_+^o}{z_+ \nu_+} - \frac{s_o c}{n c_o} \right) \left(1 + \frac{d \ln f_\pm}{d \ln c} \right) \nabla \ln c \tag{2}$$

In lithium batteries, one usually selects the reference electrode to be lithium metal, and a 1:1 binary electrolyte is generally used. Then $s_o = s_- = 0$, $s_+ = -1$, $\nu_+ = n = 1$, and $\nu = 2$, and the above equation reduces to

$$\nabla \Phi_2 = -\frac{i_2}{\kappa} + \frac{2RT}{F} \left(1 - t_+^o \right) \left(1 + \frac{d \ln f_\pm}{d \ln c} \right) \nabla \ln c \tag{3}$$

?? check sign

The second term on the right side accounts for concentration overpotential. In porous media, the conductivity is corrected by the Bruggeman relation, $\kappa = \epsilon^{1.5} \kappa_\infty$, where κ_∞ is the conductivity of the bulk electrolyte.

Since only potential differences, and not absolute potentials, are measurable, Φ_2 has an arbitrary datum as a boundary condition. Ref. [11] sets $\Phi_2 = 0$ at the positive electrode-current collector interface.

3.2 Potential in the solid

The potential in the porous solid (electrode) phase is determined from Ohm's Law:

$$I - i_2 = -\sigma \nabla \Phi_1 \tag{4}$$

where $I - i_2 = i_1$ is the current in the electrode phase and the electronic conductivity of the bulk solid is corrected for the volume fraction of the electrode by the Bruggeman relation, $\sigma = \sigma_\infty (1-\epsilon)^{1.5}$. σ_∞ is the conductivity of the nonporous composite (active + conductive filler + binder) electrode.

This equation has one boundary condition in each electrode region. For galvanostatic operation, the boundary condition in the negative electrode is $i_2 = I$ at the negative electrode-separator interface, and in the positive electrode it is $i_2 = 0$ at the positive electrode-current collector interface. When all 6 governing equations are solved simultaneously, these boundary conditions enforce the requirement that the potential in the solid phase be adjusted so that the total amount of reaction across the electrode is equal to the applied current. For potentiostatic operation, $\Phi_1 \mid_{x=L_-+L_s+L_+} - \Phi_1 \mid_{x=0} = V$.

3.3 Transport in the electrolyte

3.3.1 Dilute solution theory

Dilute solution theory is not often used in the treatment of lithium batteries, because most electrolytic solutions used in lithium batteries exhibit concentrated behavior. However, dilute solution theory becomes useful for cases such as the examination of side reactions such as redox shuttles for overcharge protection, because concentrated solution theory becomes more complicated when there are more than three species (anion, cation, and solvent) in solution.

The basic flux equation for dilute solution theory is

$$\frac{N_i}{\epsilon} = -D_i \nabla c_i - z_i u_i F c_i \nabla \Phi + \frac{\mathrm{c_i v}_o}{\epsilon} \tag{5}$$

where N_i is the flux of species i across the apparent area of the electrode, N_i/ϵ is the flux through the region occupied by the solution phase, and the mobility is usually related to the diffusivity by the Nernst-Einstein equation, $D_i = RTu_i$. Dispersion can be included in this equation if solvent velocity in the electrodes is significant[1], but this is rarely the case in the thin cell configurations commonly used in lithium batteries. The effective diffusivity used in this equation includes effects of tortuosity.

The electrostatic potential in solution is then obtained by recognizing that the current density in solution is due to the net flux of ions:

$$\nabla \Phi_2 = -\frac{i_2}{\kappa} - \frac{\epsilon F}{\kappa} \sum z_i D_i \nabla c_i \tag{6}$$

In dilute solution theory, this equation is used instead of equation 3.

3.3.2 Concentrated solution theory

Concentrated solution theory includes interactions among all species present in solutions whereas dilute solution theory assumes that ions interact only with the solvent and not with other ions. In addition, dilute solution theory assumes that all activity coefficients are unity. There is substantial evidence that both liquid and especially polymer electrolytes used in lithium batteries exhibit concentrated behavior[12, 13, 14, 15].

The foundation of concentrated solution theory is the Stefan-Maxwell multicomponent diffusion equation[16, 17],

$$c_i \nabla \mu_i = RT \sum_j \frac{c_i c_j}{c_T \mathcal{D}_{ij}} (\mathrm{v}_j - \mathrm{v}_i) \tag{7}$$

where v_i is the velocity of species i in the interstitial solution phase with respect to a reference velocity and $\mathcal{D}_{ij}$ express the pairwise frictional interactions among species. This expression relates the driving force for species motion to all of the pairwise interactions among the components.

With the selection of a reference velocity, the Stefan-Maxwell equations can be inverted to yield flux equations. We choose the reference velocity to be that of the solvent and consider the case of a binary electrolyte, for which flux equations can be obtained for both the cation and the anion. Since usually only the cation reacts in lithium batteries, the equations are made simpler later on if we focus only on a mass balance for the anion. By electroneutrality, the mass balance for the anion must be identical to that for the cation. The flux equation for the anion obtained from inverting the Stefan-Maxwell equations is

$$N_- = -\frac{\nu_- \mathcal{D}}{\nu RT} \frac{c_T}{c_o} \epsilon c \nabla \mu_e + \frac{i_2 t_-^o}{z_- F} + c_- \mathrm{v}_o \tag{8}$$

where the diffusion coefficient of the electrolyte, $\mathcal{D}$, and the transference number t_-^o with respect to the solvent are related to the diffusion coefficients $\mathcal{D}_{ij}$ by

$$\mathcal{D} = \frac{\mathcal{D}_{o+} \mathcal{D}_{o-} (z_+ - z_-)}{z_+ \mathcal{D}_{o+} - z_- \mathcal{D}_{o-}} \tag{9}$$

$$t_-^0 = 1 - t_+^o = \frac{-z_- \mathcal{D}_{o-}}{z_+ \mathcal{D}_{o+} - z_- \mathcal{D}_{o-}} \tag{10}$$

From porous electrode theory, the mass balance for the anion is

$$\epsilon \frac{\partial c_-}{\partial t} = -\nabla \cdot N_- + a j_- \tag{11}$$

where aj_- is the reaction rate of the anion per unit volume. This equation involves averaging over a region small with respect to the overall dimensions but large compared to pore structure[18, 1]. The idea is to capture the essential behavior of a composite medium without having to specify the shape and position of every pore in the porous electrode. Because porous electrode theory treats the electrode as a superposition of solid and solution phases, the electrochemical reaction enters the equation as a homogeneous term rather than as a boundary condition. Substituting in the flux equation, one obtains

$$\epsilon\frac{\partial c}{\partial t} = \nabla\cdot\epsilon D\left(1-\frac{d\ln c_o}{d\ln c}\right)\nabla c + \frac{t_-^o\nabla\cdot i_2 + i_2\cdot\nabla t_-^o}{z_+\nu_+F} - \nabla\cdot c\mathrm{v}_o + aj_- \tag{12}$$

which was obtained using the relations $c = \frac{c_-}{\nu_-}$, $\mu_e = \nu_+\mu_+ + \nu_-\mu_- = \mu_e^\Theta + \nu RT\ln\gamma_\pm m$ (definition of chemical potential for the salt in the electrolyte), $m = \frac{c}{c_oM_o}$ (conversion between molality and concentration), and $z_+\nu_+ = -z_-\nu_-$ (charge balance for a binary electrolyte). The chemical diffusion coefficient, D, is the property commonly measured for a binary electrolyte, and is related to the diffusion coefficient of the electrolytes, $\mathcal{D}$, by

$$D = \mathcal{D}\frac{c_T}{c_o}(1+\frac{d\ln\gamma_\pm}{d\ln m}) \tag{13}$$

Convection in the electrolyte is usually negligible[19]; then the term involving v_o can be neglected. $z_+\nu_+$ is 1 for most salts used in lithium batteries, and j_- is zero in the absence of side reactions. If there is no change in volume in the electrode (*i.e.*, the active material does not change in volume as it reacts, and there is no side reaction that changes the electrode porosity), then no mass balance for the solvent is needed. We discuss volume changes in section 4.8. In the separator, $\nabla\cdot i_2 = 0$, and ϵ is the volume fraction of electrolyte in the separator (equal to 1 if no inert separator material, such as glass felt or porous polyethylene, is used).

The form of the mass balance presented in equation 12 is the most convenient for treating multiple reaction pathways, such as arise when treating side reactions, double-layer capacitance, or particle-size distributions (see section 4). In these situations, $\nabla\cdot i_2$ may have a complicated relationship to the local reaction rates, but the mass balance in the form of equation 12 remains unchanged. A current balance for calculating $\nabla\cdot i_2$ is discussed in section 3.6.

The boundary condition at a lithium foil electrode is that the flux of the anion is zero. Then diffusion of the anion is balanced by migration:

$$\epsilon\frac{\partial c}{\partial x}\,|_{x=0} = -\frac{I(1-t_+^o)}{FD},\ \text{foil electrode} \tag{14}$$

The flux of the salt is zero at the current collectors of porous electrodes, where all of the current is in the matrix phase:

$$\frac{\partial c}{\partial x} = 0 \,\text{at}\, x = L_- + L_s + L_+ \,\text{and}\, x = 0, \text{ porous electrodes} \tag{15}$$

The concentration and flux are continuous at the interface between the separator and a porous electrode.

When ion-exchange polymers (ionomers), for which $t_+^o = 1$, are used for the electrolyte, no mass balance equation is needed, because the concentration of cations is fixed by the concentration of immobile anions. In this case, only one transport property, the conductivity, is needed, as opposed to the three transport properties (κ, D, and t_+^o) needed to characterize concentrated solutions and the two transport properties (D_+ and D_-) used for dilute solutions. The transference number for cations is equal to 1 in ionomers.

3.4 Transport in the solid

The porous solid phase in most lithium batteries contains particles which can be modeled as spheres. The active material of the insertion electrodes used in most lithium-ion batteries consists of mobile cations, mobile electrons, and immobile host matrix. If one neglects the effects of stress and anisotropic diffusion, then transport of lithium ions can be described as above, yielding

$$\frac{\partial c_s}{\partial t} + \nabla \cdot (c_s \mathrm{v}_o) = \nabla \cdot \left[D_s \left(1 - \frac{d \ln c_o}{d \ln c_s} \right) \nabla c_s \right] - \frac{i \cdot \nabla t_+^o}{z_+ \nu_+ F} \tag{16}$$

Since the active material is generally a good electronic conductor, $t_-^o \approx 1$ and the last term can be neglected. If volume changes in the solid are negligible, then v_o and $\frac{d \ln c_o}{d \ln c_s}$ are zero, and the mass balance reduces to

$$\frac{\partial c_s}{\partial t} = \frac{1}{r^2} \frac{\partial}{\partial r} \left(D_s r^2 \frac{\partial c_s}{\partial r} \right) \tag{17}$$

with the boundary conditions

$$\frac{\partial c_s}{\partial r} |_{r=0} = 0 \text{ and } - D_s \frac{\partial c_s}{\partial r} |_{r=R} = j_{Li^+,f} \tag{18}$$

and initial condition $c_s(t = 0, r) = c_s^o$.

From the boundary condition at the edge of the particle, one sees that any changes to calculations of the reaction rate will be coupled to the mass balance in the solid.

Under this framework, diffusion within a solid particle is considered, but diffusion between adjacent solid particles is neglected. Since the length scale between particles is much larger than the length scale within a particle, this simplification should not introduce much error.

3.5 Reaction rate

A rate equation is needed to determine the dependence of the local electrochemical reaction rate on concentration and potential. Usually, the Butler-Volmer rate equation is used

$$i_n = i_0 \left[\exp\left(\frac{\alpha_a F(\phi_1 - \phi_2 - U)}{RT} \right) - \exp\left(-\frac{\alpha_c F(\phi_1 - \phi_2 - U)}{RT} \right) \right] \tag{19}$$

The surface overpotential, $\phi_1 - \phi_2 - U$, is the deviation from the thermodynamic potential difference between the solid and solution at the existing surface concentrations. U is the open-circuit potential of the solid material evaluated at the surface concentration of the solid with respect to a hypothetical lithium reference electrode in solution just outside the diffuse part of the double layer, at the same local electrolyte concentration, and is a function of solid concentration in insertion electrodes. Thus, U must be specified as a function of intercalant concentration but not as a function of electrolyte concentration. This equation is coupled to the equations 3 and 4 for potential in the solid and electrolyte, and sets the surface overpotential with respect to the local potential in solution and potential in the solid required to force the reaction.

The magnitude and dependence on solid concentration of U vary considerably among different insertion materials. The shape of the open-circuit-potential profile has a large effect upon the simulation results, and accurate data for this property measured with respect to a lithium reference electrode are very important, especially when one is comparing full-cell-sandwich simulations with experimental data. Verbrugge and Koch[20] fit the open-circuit potential of carbon fiber by using a polynomial expansion for the excess Gibbs free energy (Wohl expansion), and this expansion matches the measured U well for the disordered carbon. For cases in which such an expansion does not capture the effects of ordering in the active material, we recommend that a careful emperical fit to measurements of the open-circuit potential be used in the simulations.

The anodic and cathodic transfer coefficients, α_a and α_c, correspond to the fractions of the applied potential which favor the anodic and cathodic directions of the overall reaction, respectively. The dependence of exchange current density on concentration is given by

$$i_0 = i_{0,ref} \prod_i \left(\frac{c_i}{c_{i,ref}} \right)^{\gamma_i} \tag{20}$$

where $i_{0,ref}$ is the exchange current density measured at the reference concentrations $c_{i,ref}$. For an elementary step, $\gamma_i = \beta s_i$ if species i is a reactant in the anodic direction and $\gamma_i = (\beta - 1) s_i$ if species i is a reactant in the cathodic direction, where s_i is the stoichiometric coefficient (positive for anodic products) and β is the symmetry factor representing the fraction of the applied potential that favors the cathodic direction of the elementary step[10]. For complex reactions involving multiple elementary steps, γ_i, α_a, and α_c may be complicated functions of the symmetry factors for each elementary step, and γ_i may differ from α_a and

α_c[10]. Presently, reaction mechanisms at electrode interfaces, particularly in the presence of the solid-electrolyte interphase, are not understood in great detail. Fortunately, the rapid kinetics of electrodes used in lithium batteries reduces the importance of the exact reaction mechanism in the battery model. In the absence of more detailed information about reaction mechanisms, the reaction can be assumed to be first order in lithium-ion concentration in the electrolyte and lithium concentration in the insertion electrode, which means that α_a, α_c, γ_{Li_s}, and γ_{Li^+} are equal to 0.5. While the assumption that $\gamma_{Li^+} = \alpha_a$ is not necessarily true for a complex reaction mechanism, such an assumption is commonly used in the literature and will be used in the following equations.

At a lithium foil electrode or at a phase-change electrode, the solid concentration is constant. At an insertion electrode involving the reaction

$$\mathrm{Li}\Theta_s \rightleftharpoons \mathrm{Li}^+ + \Theta_s + e^- \tag{21}$$

the exchange current density is given by

$$i_0 = F(k_a)^{\alpha_c}(k_c)^{\alpha_a}(c_{s,max} - c_s)^{\alpha_a}(c_s)^{\alpha_c}(c)^{\alpha_a} \tag{22}$$

where $(c_{s,max} - c_s)$ is the concentration of unoccupied sites in the insertion material. Thus, the exchange-current density tends to zero as the solid concentration approaches either 0 or $c_{s,max}$.

Some models[2] of polymer electrolytes have treated the polymer as having a fixed number of sites c_{max} for lithium ions on the polymer lattice. The reaction, *e.g.,* at the lithium foil electrode, was then expressed as

$$\mathrm{Li} + \Theta_p \rightleftharpoons \mathrm{Li}^+\Theta_p + e^- \tag{23}$$

leading to the following expression for the exchange current density:

$$i_0 = F(k_a)^{\alpha_c}(k_c)^{\alpha_a}(c_{max} - c)^{\alpha_c}(c)^{\alpha_a} \tag{24}$$

There is not much experimental evidence for or against this hypothesis, given the uncertainties in the nature of the polymer-solid interface. However, because exchange-current densities for most electrodes used in lithium batteries tend to be high, the precise nature of the kinetic rate constants is not of large importance.

Since the reaction-rate equation is algebraic, it requires no boundary condition.

3.6 Current balance

The rate of production of species i per unit volume is aj_i. In the most general case, a species can be produced by heterogeneous electrochemical reactions or homogeneous chemical reactions:

$$aj_i = aj_{i,n} + \sum_k s_{i,k} r_k \tag{25}$$

where $aj_{i,n}$ is the net flux of species i due to electrochemical reaction normal to the active material surface and r_k is the rate of the kth chemical reaction. For an electrochemical reaction expressed by

$$\sum_i s_i M_i^{z_i} \rightarrow ne^- \tag{26}$$

the faradaic reaction of species i is related to the rate of electrochemical reaction by

$$aj_{i.n} = -\frac{as_i}{nF} i_n \tag{27}$$

and i_n is determined by a kinetic relationship as described in the previous section.

By electroneutrality, a current balance relates the divergence of the current to the net pore-wall flux due to reaction:

$$\nabla \cdot i_2 = ai_n \tag{28}$$

For the case of multiple electrochemical reactions,

$$\nabla \cdot i_2 = \sum_l a_l i_{n,l} \tag{29}$$

and

$$aj_{i.n} = -\sum_l \frac{as_{i,l}}{nF} i_{n,l} \tag{30}$$

The boundary condition on this equation is that the divergence of the current is zero in the separator.

3.7 Energy balance

An energy balance is required to calculate the heat generated by the cell and the temperature changes in a cell or stack of cells. In this section, we discuss the equations needed to calculate the heat generated by the cell. Since most lithium cells are very thin (less than 300 μm thick), temperature gradients perpendicular to the electrodes are neglegible, allowing peltier heats of individual electrodes, transport entropy, and thermal diffusion to be neglected. The heat generation therefore need not be calculated as a function of position across an individual cell. Once known, this heat generation can be inserted into a standard heat transfer equation, including conduction, convection, and radiation as appropriate for the battery geometry, to calculate temperature changes across a tall cell or battery stack. Such

models are generally concerned with temperature gradients in two- or three-dimensions. We review multidimensional modeling in section 4.11. Newman [21] discusses issues that arise when the temperature varies perpendicular to the electrodes.

The form of the energy balance commonly used in modeling batteries is

$$\dot{Q} = I\left(V - U + T\frac{\partial U}{\partial T}\right) + C_p\frac{dT}{dt} \tag{31}$$

where $\dot{Q}$ is the rate of heat transferred to the system from its surroundings. This equation states that heat is generated due to the presence of resistance to the passage of current $I(V-U)$ and due to reversible heat effects $I(T\partial U/\partial T)$. This equation assumes that no heat is generated by relaxation after the current is turned off. Several authors have compared heat-generation predictions using this energy balance for a single cell to experiment[22, 23].

While this form of the energy balance is accurate enough for many cases of interest, it does ignore several facets of heat generation. Bernardi *et al.*[24] describe a more general form of the energy balance which includes heats of multiple reactions, mixing, phase change, and changes in heat capacity. They use this model to describe the heat generation in a LiAl | molten LiCl, KCl | FeS cell, including the effects of two reaction steps in the FeS electrode, precipitation of LiCl, and heat of mixing in the molten salt electrolyte. Heat required to form concentration gradients during the passage of current is released upon relaxation of those gradients after interruption of the current. If the second derivative of the enthalpy of the electrolyte with respect to mole fraction of one component of the electrolyte is positive, then the heat released during relaxation is exothermic.

Rao and Newman[25] present a form of Bernardi *et al.*'s energy balance which is convenient for examining heat-of-mixing effects across insertion compounds, in which the open-circuit potential varies with state of charge:

$$\dot{Q} = IV + \int \sum_l a i_{n,l}(x)\left(U_l\left(c_s(x)\right) - T\frac{\partial U_l\left(c_s(x)\right)}{\partial T}\right)dx + C_p\frac{dT}{dt} \tag{32}$$

where c_s is the local lithium concentration in the solid averaged over the cross-sectional area of the electrode, the integral is over the entire cell, and the reaction rate i_n is positive for an anodic reaction. This equation reduces to equation 31 only for the case of a uniform reaction rate or constant U_H, where the enthalpy potential is given by $U_H = U - T\frac{\partial U}{\partial T}$. Because it involves the local reaction rate, rather than the overall applied current, it can be used to treat heat effects of self-discharge and the formation and relaxation of concentration gradients across the insertion electrode. While it treats heat of mixing across the electrode, it does not include heat of mixing within the electrolyte or within individual particles of the active material[26]. Since all three sources of heat of mixing are of comparable magnitude, it is perhaps not prudent to include only one of them in the energy balance. For electrolyte and electrode materials with transport properties sufficiently high to be of interest for commercial

batteries, with their typically thin cells and small particles, the heat of mixing terms will be small relative to resistive and entropic terms[26].

One of the characteristic features of lithium-ion batteries is the use of insertion compounds as active materials. Ordering effects of lithium on the insertion lattice cause the entropy of reaction, $T\partial U/\partial T$, to be of significant magnitude and to vary strongly, even changing sign, with state of charge[27]. Knowledge of the entropy of reaction as a function of state of charge therefore is required for accurate prediction of heat generation from batteries containing insertion electrodes.

Physical properties such as κ, i_0, and D generally display an Arrhenius dependence on temperature. Therefore, as the temperature of the battery increases, these properties increase, the resistance of the cell decreases, and the rate of heat generation decreases. These effects tend to even out temperature distributions across a stack compared to what would be predicted using constant physical properties[28]. In opposition to this trend, the rate of heat generation from side reactions may increase with increasing temperature[29].

3.8 Solving the governing equations

The previous sections describe the six equations (equations 3, 4, 12, 17, 19, and 28) necessary to describe the electrochemical performance of the cell. Solving these equations yields the dependent variables c, c_s, Φ_1, Φ_2, i_2, and j. The governing equations involve three ordinary differential equations, two partial differential equations, and one algebraic equation. If explicit calculation of both Φ_1 and Φ_2 is not needed, they may be combined into one variable, $\eta = \Phi_1 - \Phi_2$. If explicit calculation of both j and i_2 is not required, then equations 19 and 28 may be combined into one equation.

In all but the most simplified cases, the coupled governing equations must be solved numerically. Use of variable physical properties and/or Butler-Volmer or Tafel kinetics makes the governing equations nonlinear. Several different numerical techniques have been used in the literature, including finite difference with control volume formulations for the mass and charge balances[2, 3, 30], finite elements[6, 31], and the method of lines[32, 33]. Time derivatives are handled using Crank-Nicholson formulations or higher-order variations of implicit methods.

For this type of model based upon the fundamental laws of transport, kinetics, and thermodyanmics, a large number of physical properties is required, as listed in table 1. These properties may all be functions of composition and temperature, in particular, U, κ, D, t_+^o, and D_s. A summary of the experiments required to measure the parameters needed for the model is given by Doyle and Newman[34]. A full-cell sandwich model of a lithium battery using the above equations was first presented by Doyle, Fuller, and Newman[2, 11]. This model has been validated several times by comparison with experimental discharge and charge data over a wide range of current densities for various lithium and lithium-ion cell chemistries[35, 36].

4 Special situations

4.1 Transport in insertion electrodes

Transport in insertion compounds is perhaps one of the easiest solid transport situations to model, because there is no phase change or generation of new product compounds, and volume changes are generally negligible. Therefore, the morphology of the electrodes is relatively constant, and only diffusion need be considered.

4.1.1 Constant diffusion coefficient

If the solid diffusion coefficient can be approximated as a constant, then equation 17 is a linear partial differential equation. Then the concentration in the particle resulting from a time-varying rate of reaction at the surface can be obtained by superposing the concentration changes resulting from simple step changes in concentration at the surface. Each step change is initiated at a different time t_n, and the effect of that step at future times is damped as the response decays. In the limit as the time step goes to zero, the flux into the particle can be expressed by Duhamel's superposition integral[37, 38]

$$\frac{\partial c_s}{\partial r}(R,t) = \int_0^t \frac{\partial c_s}{\partial t}(R,\delta)\frac{\partial \overline{c}_s}{\partial r}(R,t-\delta)d\delta \tag{33}$$

where $\overline{c}_s(r,t)$ is the dimensionless concentration resulting from a unit step change in concentration at the surface of the particle. We see that calculation of the flux into the particle requires only knowledge of the history of the surface concentration of the particle, and we do not need to keep track of the concentration within the particle. This simplification saves computer memory and computation time.

This initial-value type integral equation can be calculated numerically using the method presented by Wagner[39] and Acrivos and Chambre[40]. The time-derivative of c_s can be approximated numerically by $\frac{\partial c_s}{\partial t} = \frac{c_{s,j+1}-c_{s,j}}{\triangle t}$. Substituting into equation 33 and discretizing time into time steps t_n yields:

$$\frac{\partial c_s}{\partial r}(R,t_n) = \frac{(c_{s,n}-c_{s,n-1})}{\triangle t}A_1 + \sum_{j=0}^{n-2}\frac{(c_{s,j+1}-c_{s,j})}{\triangle t}A_{n-j} \tag{34}$$

where

$$\frac{D_s}{R}A_n = a(t_n) - a(t_{n-1}) = \frac{D_s}{R}\int_0^{t_n}\frac{\partial \overline{c}_s}{\partial r}(R,\xi)d\xi - \frac{D_s}{R}\int_0^{t_{n-1}}\frac{\partial \overline{c}_s}{\partial r}(R,\xi)d\xi \tag{35}$$

The summation in equation 34 is divided to illustrate that the summation can be stored and updated at each time step.[1] The Laplace transform can be used to obtain series expansions

[1]Equation 34 often has been presented in dimensionless form[2, 41]. To avoid confusion, we present it here in dimensional form.

for $a(t)$. At long times,

$$a(\tau) = \frac{2}{\pi} \sum_{n-1}^{\infty} \frac{1}{n^2} \left[1 - \exp\left(-n^2\pi^2\tau\right)\right] \tag{36}$$

At short times,

$$a(\tau) = -\tau + 2\left(\frac{\tau}{\pi}\right)^{0.5} \left\{1 + 2\sum_{n=1}^{\infty}\left[\exp\left(\frac{-n^2}{\tau}\right) - n\sqrt{\pi/\tau}\mathrm{erfc}\left(n/\sqrt{\tau}\right)\right]\right\} \tag{37}$$

where τ is dimensionless time defined as $\tau = tD_s/R^2$. Doyle[41] states that evaluating three terms of the short-time solution or five terms of the long-time solution provides sufficient accuracy. The long-time solution is used when τ is greater than 0.06. The above equations were derived for spherical particles. Doyle also provides series solutions for $a(\tau)$ for other shapes of particles such as parallel slabs and cylindrical rods (neglecting edge effects and considering only 1-D transport in each geometry).

4.1.2 Variable diffusion coefficent

If the variation of the solid diffusion coefficient with lithium concentration is significant, then the diffusion equation is nonlinear and the above simplification does not apply. For an electrode composed of spherical particles, a pseudo-two dimensional approach is required, in which the radial diffusion equation (equation 17) is solved at each mesh point across the porous electrode. A set of radial nodes is then required to compute the radial solid concentration profile at each linear position in the electrode. Note that equation 17 is derived using the gradient in chemical potential, and assumes only that volume changes are negligible and that all current is carried by electrons in the solid phase. The chemical diffusion coefficient, D_s, used in equation 17 is related to the binary diffusion coefficient derived from the Stefan-Maxwell equations, $\mathcal{D}$ (also called the binary interaction parameter), by the relationship presented earlier (equation 13) for concentrated solutions:

$$D_s = \mathcal{D}\frac{c_T}{c_o}(1 + \frac{d\ln\tilde{\gamma}_{\pm}}{d\ln\Theta}) \tag{38}$$

Following convention in the literature, we have changed here from a molal scale to a fractional occupancy scale, defined by $\mu_s = \mu_s^{\star} + \nu RT\ln\tilde{\gamma}_{\pm}\Theta$, where $\Theta = c_s/c_{s,max}$ is the fraction of lithium sites in the lattice which are occupied. Then in equation 16, the term $1 - \frac{d\ln c_o}{d\ln c_s}$ should be replaced by $1 - \frac{d\ln c_{s,max}}{d\ln c_s}$. For insertion compounds, the thermodynamic factor is related to the open-circuit potential by[2]

[2]Some authors define the thermodynamic factor as $1 + \frac{d\ln\gamma_{\pm}}{d\ln\Theta} = -\Theta\frac{F}{RT}\frac{\partial U}{\partial\Theta}$ and then combine the $(1-\Theta)$ term with the binary interaction parameter.

$$1 + \frac{d \ln \tilde{\gamma}_{\pm}}{d \ln \Theta} = -\Theta(1-\Theta)\frac{F}{RT}\frac{\partial U}{\partial \Theta} \tag{39}$$

While $\mathcal{D}$ may vary less with concentration than does the chemical diffusion coefficient, McKinnon and Haering[42] provide a theoretical basis for how $\mathcal{D}$ varies with concentration, depending on attractive and repulsive interactions in the lattice. There is a vast experience with materials for which $\mathcal{D}$ varies with concentration[43, 44, 45]. The assumption that $\mathcal{D}$ is independent of lithium concentration may be valid for some electrode materials, such as carbon fiber[46]. However, since this assumption has no theoretical basis, it should be used only with caution and verified with measurements of the diffusion coefficient as a function of concentration.

While use of a variable diffusion coefficient increases simulation accuracy, it also increases simulation time by up to an order of magnitude, depending on the number of radial nodes used. Therefore, in some cases it is desirable to use a constant diffusion coefficient. This constant should be some average value of the true variable diffusion coefficient. The question arises, what average value of the diffusion coefficient to use for a material that exhibits a diffusion coefficient that varies with state of charge? Paxton and Newman[47] present one method for selecting an average diffusion coefficient. The procedure involves setting up a separate simulation for a single spherical particle with variable diffusivity and performing many simulations at different values of dimensionless surface reaction rate, $\Phi = \frac{j_n R}{D_o c_{s,max}}$, where D_o is the maximum diffusivity, $c_{s,max}$ is the maximum solid concentration, j_n is the surface flux due to reaction, and R is the radius of the spherical particle. The simulations are then repeated for constant diffusivity, and the value of D_s which gives the best match to surface concentration predicted with the variable diffusivity is selected at each value of Φ. For small values of Φ, variations in the solid diffusion coefficient have negligible effects on cell performance. In this manner, one obtains a relationship between the best value of diffusivity to use and Φ. One can then use this relationship in the full cell simulation. For the full cell simulation, Φ is calculated assuming a uniform reaction rate: $\Phi = \frac{iR^2}{3D_o c_{s,max} LnF\epsilon_{active}}$, where L is the electrode thickness and ϵ_{active} is the volume fraction of active material. Paxton and Newman compare two alternatives for defining "best match".

Verbrugge and Koch describe how to scale the radial dimension when formulating the radial diffusion equation to improve numerical simulations over a wide range of time scales[20]. Mao and White[48] present a method for arranging the matrix when solving pseudo-two dimensional problems that reduces computation time.

4.2 Transport and volume change in phase-change electrodes

Several phase-change electrodes are currently being researched for use in lithium-ion batteries, such as lithium-tin and other binary and intermetallic lithium alloys for negative electrodes, and $LiFePO_4$ and variants thereof for positive electrodes. In these materials, the

reaction occurs as a moving front through the particle of active material rather than as diffusion down a continuous concentration gradient as in insertion compounds. The new phase must be nucleated at the surface of grains before the phase can propagate through a grain, resulting in a nucleation overpotential. The nucleation overpotential is observed as a sharp dip and then rise in the cell potential at the beginning of discharge. The phase-propagation process can be treated with a shrinking-core model, as described in Appendix C of ref. [49] and as applied in the case of LiAl[19].

This type of phase-change reaction is distinct from the dissolution-precipitation reaction which occurs in the Pb, PbO_2, Ag, and Cd electrodes. In a dissolution-precipitation reaction, one solid phase (*e.g.* Pb) dissolves electrochemically (*e.g.* to form Pb^{2+}), combines with an ion in solution, and the product precipitates (*e.g.* $PbSO_4$). Methods for modeling mass transfer and nucleation kinetics in dissolution-precipitation reactions have been described [18, 50, 51, 52, 53, 8].

Some of the materials recently being considered for use as positive electrodes, such as $LiFePO_4$, are actually insulators rather than electronic conductors. In this case, the assumption that the transference number of electrons is unity is not valid, and semiconducting effects may need to be considered. Treatment of semiconducting effects in electrodes has been reviewed in the case of the nickel hydroxide electrode[54, 55] and photovoltaic electrodes[56, 57].

4.3 Nonporous insertion electrodes

Nonporous electrodes are of interest for thin-film microbatteries, especially all-solid-state batteries, and for measurements of the solid diffusion coefficient and exchange-current density, since these measurements require knowledge of the surface area. In the nonporous geometry, no electrolyte, binder, or filler is present in the electrode. Then only two governing equations apply. The electrode has a planar geometry. Let $x = 0$ be the electrode-current collector interface, and $x = L$ be the position of the electrode-separator interface. The first governing equation is Ohm's law in the solid,

$$I = -\sigma \nabla \Phi_1 \tag{40}$$

with the boundary condition

$$I = i_0 \left[\exp\left(\frac{\alpha_a F \eta_s}{RT}\right) - \exp\left(\frac{-\alpha_c F \eta_s}{RT}\right) \right] \tag{41}$$

where η_s is the surface overpotential as defined earlier,

$$\eta_s = \Phi_1(x = L) - \Phi_2(x = L) - U(c_s(x = L)) \tag{42}$$

and we see that this boundary condition couples the potential in the solid to the potential in solution and the surface concentration in the electrode. If σ is a constant, then equation 40 can be integrated directly to yield $\Phi_1(L) - \Phi_1(0) = -\frac{IL}{\sigma}$.

The second governing equation is the planar diffusion equation for lithium transport in the solid film

$$\frac{\partial c_s}{\partial t} = \frac{\partial}{\partial x}\left(D_s \frac{\partial c_s}{\partial x}\right) \tag{43}$$

with boundary conditions

$$\frac{\partial c_s}{\partial x}\,|_{x=L} = -\frac{I}{FD_s} \text{ and } \frac{\partial c_s}{\partial x}\,|_{x=0} = 0 \tag{44}$$

and initial condition $c_s(x, t = 0) = c_s^o$.

For a constant diffusion coefficient and boundary conditions of constant current (galvanostatic operation) or constant surface concentration (*e.g.,* for a potential step experiment), this equation can be integrated directly[58]. For nonconstant boundary conditions but constant diffusion coefficient, the equation can be solved using Duhamel's superposition integral[59]. With an arbitrarily variable diffusion coefficient, the equation must be solved numerically.

4.4 Particle size distribution

The battery model described above assumes that the active material in the porous electrodes exists in small spherical particles of uniform size. In a real battery, the particle size may be nonuniform. A particle size distribution is modeled numerically by categorizing the particles into size bins, and then treating each bin as a separate phase in the electrode. While each particle size has the same material properties, the particles may experience different reaction rates and thus solid-phase concentrations. The reaction rate equation 19 is computed separately for each particle size bin. The current balance then becomes

$$\nabla \cdot i_2 = \sum_l a_l i_{n,l} \tag{45}$$

where the summation is over the bins of particle sizes. Different particle size bins may have different specific interfacial areas, calculated from $a_l = 3\epsilon_l/R_l$ for spherical particles. A separate solid material balance of the form of equation 17 is written for each particle-size bin. The equations for the potential in the electrolyte and solid remain unchanged, and the mass balance in the electrolyte is unaffected if the form of equation 12 is used. The equation for the potential in the solid is unchanged because the averaging employed in porous electrode theory is over regions that include several particles. Therefore, the solid-phase potential is the same in particles of all sizes at a given position. This analysis neglects any effect of

radius of curvature on surface energy and therefore on chemical potential; this assumption is valid for particle radii of order nanometers or larger.

Darling and Newman[60] examine the effects of a particle-size distribution by considering the simplified case of binary distributions in which the volume fractions of the two particle sizes are chosen in such a way that the active-material volume fraction (and thus mass), surface area, and average particle size are the same among all the distributions examined. Thus, the only physical parameter changed in Darling and Newman's simulations is the presence of two particles sizes, thereby isolating the effect of a particle size distribution. The authors show that an electrode with a particle-size distribution, all else held constant, exhibits larger solid-phase resistance and longer relaxation times than an electrode with uniform particle size. The effect is most pronounced under conditions of nonuniform current distribution across the electrode, such as at high currents or flat dependence of the open-circuit potential on solid concentration.

Figure 2 shows the potential of the surface of the particles as a function of time during a charge and discharge of a Li | $LiMn_2O_4$ evaluated at the concentration of the surface of the particle. The concentration in the two particle sizes is identical as long as semi-infinite diffusion exists. Once the solid concentration gradients extend to the middle of the particle, restricted diffusion behavior takes over, and the concentration in the smaller particle will change faster than the concentration in the larger particle. The solid concentration overpotential (difference between actual cell potential and surface potential) is therefore larger in the larger particles. Therefore, for electrodes with the same average particle size, surface area, and volume fraction of active material, the electrode with the most nonuniform particle-size distribution will have the largest overpotential and slowest relaxation times. Another way to think of this is that, in any particle-size distribution, there must always be particles of size larger than the average, and these larger particles will always have larger resistances and time constants for diffusion. For a particle-size distribution with different surface areas, the kinetic overpotential will be larger on the particle size of smaller surface area a.

Particles of different sizes will pack differently than particles of a uniform particle size, and the packing density will affect the porosity of the electrode. Nagarajan *et al.*[61] addressed the question of how to optimize the particle-size distribution to increase electrode utilization for a 1C-rate discharge, given a correlation between packing density and particle size determined by Yu *et al.*[62] (neglecting effects of the conductive filler and binder on packing). In essence, this paper tries to optimize the electrode porosity by changing the packing density in the electrode. Nagarajan *et al.* also demonstrate how a higher fraction of smaller particles can improve electrode response to a high-current pulse discharge.

4.5 Double-layer capacitance

Double-layer capacitance is of interest when modeling ac-impedance behavior and also when simulating response to rapid current pulses. Small modifications to the current balance are required to account for charging of the double layer[63]. These modifications also appear in the mass balance equation for the electrolyte, since it includes the divergence of the current as a homogeneous consumption term. In many cases, the magnitude of the concentration change due to double-layer adsorption may be negligible, and then only the modified current balance is needed. The current balance is

$$\nabla \cdot i_2 = aF \sum_i z_i j_{i,n} \tag{46}$$

where $j_{i,n}$ is the molar flux of species i away from the electrode surface due to heterogeneous electrochemical reaction. If we are to include double-layer charging, then this flux has both faradaic and capacitive components:

$$a j_{i,n} = a j_{i,f} + a_{dl} j_{i,dl} \tag{47}$$

where here we have accounted for the possibility that the interfacial area for double layer charging may include the conductive filler and therefore be different from the interfacial area for faradaic reaction. A mass balance on the excess charge in the solution side of the double layer is

$$\frac{\partial \Gamma_i}{\partial t} = -j_{i,dl} \tag{48}$$

Since the interface as a whole is electrically neutral, a charge balance on the double layer yields

$$q = -F \sum_i z_i \Gamma_i \tag{49}$$

where q is the charge on the electrode side of the double layer (assumed to be all at the surface of the conductor). Combining equations 46, 47, 48, and 49, we have

$$\nabla \cdot i_2 = aF \sum_i z_i j_{i,f} + a_{dl} \frac{\partial q}{\partial t} \tag{50}$$

Capacitance is defined by

$$\frac{dq}{dt} = C \frac{d(\phi_1 - \phi_2)}{dt} \tag{51}$$

For lithium batteries with binary electrolytes, the faradaic flux of the anion is zero. Thus our final form of the current balance becomes

$$\nabla \cdot i_2 = aFj_{+,f} + a_{dl}C\frac{\partial(\phi_1 - \phi_2)}{\partial t} \tag{52}$$

One can show that[64]

$$j_{i,dl} = -\frac{C}{z_iF}\frac{dq_i}{dq}\frac{\partial(\phi_1 - \phi_2)}{\partial t} \tag{53}$$

where the dependence of double-layer adsorption on electrolyte concentration and temperature have been neglected. To get a mass balance for the electrolyte that includes double-layer capacitance, we substitute equations 47 and 53 into the mass balance (equation 12) to obtain

$$\begin{aligned}\epsilon\frac{\partial c}{\partial t} &= \nabla \cdot \epsilon D\nabla c - \frac{i_2}{F}\cdot\nabla t_+^o + a(1-t_+^o)j_{+,f} \\ &-a_{dl}\frac{C}{F}\left(t_-^o\frac{dq_+}{dq} + t_+^o\frac{dq_-}{dq}\right)\frac{\partial(\phi_1-\phi_2)}{\partial t}\end{aligned} \tag{54}$$

where $\frac{dq_i}{dq}$ indicates the change in surface excess concentration of species i in response to a change in the charge on the electrode. Since information about surface charges is difficult to obtain, we can assume that only cations are adsorbed. Then $\frac{dq_-}{dq} = 0$ and $\frac{dq_+}{dq} = -1$. Note that the signs of these terms, equation 53, and the last term in equation 54 are reversed if q is defined as the total charge on the solution side of the double layer, rather than on the electrode side as used here. The final mass balance is independent of this definition.

Ong and Newman[65] describe issues of casting these equations into finite-difference form and derive a characteristic time for the decay of capacitive effects upon a step change in galvanostatic current. The time constant is approximately $L^2a_{dl}C\left(\frac{1}{\kappa}+\frac{1}{\sigma}\right)$, and is on the order of 1 to 100 milliseconds for typical insertion electrodes.

4.6 Film resistance

It is well known that a passivation layer, called the solid-electrolyte interphase (SEI), forms on the surface of the negative electrode (and likely on the positive electrode to some extent as well) due to reaction with the electrolyte. This layer will add a resistance for reaction to occur. The exact nature of the SEI is not well understood. There is evidence that the film on the carbon and lithium electrodes is inhomogeneous, possibly porous, composed of more-reduced species (*e.g.* Li_2CO_3) on the side bordering the active material and less-reduced species (*e.g.* lithium alkyl-carbonates) on the side bordering the electrolyte. A model of transport and reaction in the SEI layer could be based on previous works on passivation layers formed in other systems, *e.g.,* corrosion of iron[66, 67], or it could expand upon models of the LiCl layer in lithium-thionyl chloride batteries[68, 69].

For the purposes of modeling the overall cell-sandwich behavior, it is not necessary to know the exact details of the SEI layer. Instead, one can assign some overall resistance to

the film, and include this resistance in the electrode kinetics. Given that the film is believed to consist of solid lithium salts, it is logical to model transport through the film to a first approximation by migration alone, in which case the film is analogous to a resistor in series with the reaction (no diffusion resistance in the film)[35]. The surface overpotential used in the Butler-Volmer equation should then include the potential drop across this film, so that the modified Butler-Volmer equation has the form

$$i_n = i_0 \left[\exp\left(\frac{\alpha_a F(\phi_1 - \phi_2 - U - jFR_{film})}{RT} \right) - \exp\left(\frac{-\alpha_c F(\phi_1 - \phi_2 - U - jFR_{film})}{RT} \right) \right] \tag{55}$$

The film resistance affects the reaction-rate distribution by increasing the kinetic resistance, which makes the reaction rate more uniform. There is evidence that the composition of the film depends on electrode potential, and that the film dissolves and reforms as the cell is cycled. Then it might be appropriate to consider a film resistance which varies with local potential.

In addition to the film resistance around the particles of active material, there may be a contact resistance due to imperfect contact between the electrode and the current collector[70]. This contact resistance is separate from interparticle contact resistance in the bulk of the electrode, which is included in the electrical conductivity σ of the composite electrode material. Contact resistances at the current collector would have a different effect on the current distribution than a film resistance, because this contact resistance would occur only at the boundary of the electrode rather than being distributed throughout the entire surface area of active material like the film resistance. The ohmic potential drop from the contact resistance is treated by simply subtracting $IR_{contact}$ from the cell potential.

4.7 Side reactions

Side reactions include electrolyte oxidation and reduction, lithium deposition, redox shuttles for overcharge protection, corrosion of current collectors, self-discharge, conversion of active material to inactive phases, and other degradation mechanisms, as reviewed by ref. [4]. Side reactions can affect the performance of lithium-ion cells by lowering the coulombic efficiency, creating an imbalance in the state of charge between the positive and negative electrodes, consuming cyclable lithium, increasing cell impedance, or protecting against potentially more deleterious effects of overcharge.

Side reactions can be divided into two categories for the purposes of modeling. The first category includes side reactions which do not involve or produce soluble species other than the electrolyte and solvent, and include lithium deposition and solvent oxidation to form solid products. These types of side reactions are treated with little modification to the framework developed in section 3 other than the addition of a kinetic equation for the side reaction. The second category includes any side reaction which does involve more than

three components in the solution phase, such as redox shuttles. In this case, the governing equations must be modified to add a mass balance for the new component and to include the concentration overpotential of this component.

Darling and Newman[36] describe the methodology for modeling the first category of side reactions, in which the only species in the solution phase are the electrolyte and solvent. The side reaction is modeled by adding a second reaction to the current balance:

$$\nabla \cdot i_2 = a_m i_{n,m} + a_s i_{n,s} \tag{56}$$

where $i_{n,m}$ is the current flux due to the main reaction (lithium insertion) and $i_{n,s}$ is the current flux due to the side reaction. $i_{n,s}$ could be the sum of multiple side reactions. Here Darling and Newman have allowed for the possibility that the surface area upon which the side reaction occurs could be different from that of the main reaction. For example, electrolyte oxidation may occur on the surface of the conductive filler, whereas the main reaction occurs only on the surface of the active material. The effects of the side reaction are coupled to the mass balance in the solid and in the electrolyte, in that $\nabla \cdot i_2$ appears in the electrolyte mass balance, equation 12, and $i_{n,m}$ determines the flux of lithium into the solid. The total current in the cell is determined by boundary conditions such as galvanostatic or potentiostatic operation. Note that it is possible for $i_{n,m}$ and $i_{n,s}$ to have opposite signs. For example, self-discharge on the positive electrode could occur by coupling a side reaction, *e.g.,* $\mathrm{S} \rightarrow \mathrm{S}^+ + e^-$, with the main reaction $\mathrm{Li}^+ + e^- + \Theta_s \rightleftharpoons \mathrm{Li}\Theta_s$. The net current could then be zero while the state of charge of the electrode decreased due to self-discharge.

Like the main reaction, the side reaction can be described by the Butler-Volmer equation,

$$i_{n,s} = i_{0,s}\left[\exp\left(\frac{\alpha_{a,s}F}{RT}\eta_{s,s}\right) - \exp\left(-\frac{\alpha_{c,s}F}{RT}\eta_{s,s}\right)\right] \tag{57}$$

where the surface overpotential for the side reaction is defined as

$$\eta_{s,s} = \phi_1 - \phi_2 - U_s - F j_s R_{film} \tag{58}$$

where U_s is the reversible thermodynamic potential of the side reaction defined with respect to a lithium reference electrode at the same solution composition. U_s can be specified as a function of electrode composition or temperature if such information is available. Computation can be simplified somewhat by assuming that the side reaction is irreversible or the reversible potential of the side reaction is much different from the electrode potential (and therefore the Tafel approximation can be used), or that the rate constant of the side reaction is very large and the overpotential is small (and therefore linear kinetics can be used). Tafel kinetics may be more appropriate for electrolyte degradation reactions, whereas linear kinetics may be appropriate for lithium deposition[4]. For irreversible reactions, a reversible potential is not really defined and does not appear independently in the kinetic expression.

For example, if the Tafel approximation is used, then, *e.g.,* for an anodic reaction,

$$i_{n,s} = i_{0,s} \exp\left(\frac{\alpha_{a,s} F(\phi_1 - \phi_2 - U_s - j_s F R_{film})}{RT}\right) \tag{59}$$

$$= i_{0,s} \exp\left(\frac{-\alpha_{a,s} F U_s}{RT}\right) \exp\left(\frac{\alpha_{a,s} F(\phi_1 - \phi_2 - j_s F R_{film})}{RT}\right)$$

and we see that U_s can be incorporated into the exchange current density for the side reaction, and is not measured separately.

If the rates of side reactions on the two electrodes are different, then the total flux of lithium into one electrode will not be equal to the total flux of lithium out of the other electrode. An imbalance of the state of charge between the positive and negative electrodes will result. This imbalance effectively leads to a loss of cyclable capacity.

Arora *et al.*[71] use the equations presented above to simulate lithium metal deposition on carbon negative electrodes during overcharge. Lithium metal deposition will occur wherever the potential of the electrode is driven more negative than the potential of lithium metal, *i.e.,* where $\Phi_1 - \Phi_2 - U_{Li} < 0$. Since all potentials in this work are with respect to a lithium reference electrode, $U_{Li} = 0$. Such a situation might occur when there is excess positive electrode capacity, when large charging currents are used, or when the cell is charged to voltages much larger than its open-circuit potential at full state of charge. A graphical illustration of how potential varies across the carbon electrode is given in figure 3. We see that the threat of lithium deposition emerges 115 minutes into this C/2-rate charge. The surface of the deposited lithium will react with the electrolyte, causing a resistive material to coat the active material, reducing the amount of cyclable lithium in the system, and clogging pores.

Arora *et al.* use the calculated rate of side reaction to explore the its effect on film resistance. Assuming that the lithium deposition reaction occurs uniformly about the surface of the spherical carbon particles, the rate of growth of the deposit thickness $\delta_{deposit}$ is

$$\frac{\partial \delta_{deposit}}{\partial t} = -j_s \overline{V} \tag{60}$$

where $\overline{V}$ is the molar volume of the lithium deposit. They then use this deposit thickness to estimate the increase in film resistance:

$$R_{deposit}(t) = \sum_i x_i \frac{\delta_{deposit}}{\kappa_i} \tag{61}$$

$$R_{film} = R_{SEI} + R_{deposit}(t) \tag{62}$$

The summation is over the number of different layers which comprise the lithium deposit (this equation assumes the layers behave in series). For example, Arora *et al.* assume that

the lithium deposit is composed of lithium metal and Li_2CO_3, which is formed when the lithium metal reacts with the electrolyte. κ_i is the ionic conductivity, and x_i is the fraction of the total deposit thickness composed of species i. Since the exact nature of electrolyte reaction with lithium metal is not known and depends strongly on a large number of factors including impurities, x_i is taken to be an adjustable parameter. $1 - x_{lithium}$ determines what fraction of the lithium deposited is made irreversibly unavailable for further cycling in the battery. R_{SEI} is the film resistance of the SEI layer present before any overcharge reactions occur (see section 4.6).

Factors which alleviate driving the potential of the carbon surface to zero will reduce lithium deposition. These factors include increasing the negative:positive active-material mass ratio, reducing the cutoff voltage on charge, reducing the electrode thickness and particle size, and reducing the applied current density. A larger film resistance decreases the potential driving-force for lithium deposition and thus its rate. Therefore, lithium reaction with the electrolyte to form a resistive film will decrease the lithium deposition rate. A more uniform reaction rate, which could be achieved by slower reaction kinetics, lower solution resistance, or a sloping dependence of open-circuit potential on state of charge, would also reduce the rate of lithium deposition by avoiding driving the potential to zero at the electrode-separator interface before the rest of the electrode is fully charged. Finally, Arora *et al.* indicate that for a given amount of coulombs of charge reaction, the total amount of lithium deposition is reduced by using taper charging rather than galvanostatic charging.

The second category of side reactions includes those which involve species in solution other than the main electrolyte and solvent. For example, one might be interested in how Mn^{+2} from the dissolution of the positive electrode migrates to the negative electrode and plates out on the surface of the negative electrode, or in examining whether a soluble product of electrolyte reduction at the negative electrode could cause capacity fade by reacting at the positive electrode. In addition to the modification to the current balance given in equation 56, the governing equations must be modified to include a mass balance for the soluble species and to include the concentration overpotential of this species in its kinetic equation. The modifications can be handled either with full concentrated solution theory, a combination of concentrated solution theory and dilute solution theory, or by dilute solution theory alone.

Treating the system with full concentrated solution theory involves inverting the Stefan-Maxwell equations for all species involved in solution, yielding a flux equation for each species. The flux of each species is coupled to the flux of all other species in these equations, and $n(n-1)/2$ transport properties are required. In addition, the expression for the potential in solution as measured by a reference electrode, equation 2, will be modified to include gradients in chemical potential of all species present. The governing equations for an impurity ion[7, 52], impurity solvent[69], and both impurity ion and solvent[8] have been derived. A kinetic expression of the form of equation 57 for each side reaction completes the set of governing equations. U_s is defined with respect to a lithium reference electrode at the same solution composition, and all concentration overpotential is included in Φ_2.

For impurity species present in dilute concentrations, some may find it more convenient to treat the species using dilute solution theory, which accounts only for interactions of the dilute species with the solvent. Rigorously, equation 12 was derived for a binary electrolyte with no impurity species in the solution. While it is not completely rigorous to treat one species with dilute solution theory while treating the main electrolyte with equations derived from concentrated solution theory in the absence of the impurity species, the error may be small. The flux of the dilute species is given by equation 5. The mass balance for the main electrolyte remains unchanged. If Φ_2 is defined by equation 3, then U_s must be defined as a function of the concentration of the impurity species in order to include the concentration overpotential of the impurity species in the kinetic expression, equation 57. The Nernst equation, $U_s = U_s^o + RT \ln c_i/c_i^o$, is often used to account for the concentration overpotential of dilute species i. If Φ_2 is defined by equation 6, then U_s should not be defined as a function of solution composition.

The flux equation, from either concentrated or dilute solution theory, is then inserted into the material balance for the species:

$$\epsilon \frac{\partial c_i}{\partial t} = -\nabla \cdot N_i + a j_i \tag{63}$$

The reaction term aj_i includes the sum of the main and side electrochemical reactions and also chemical reactions, as indicated in equations 25 and 30. Possible chemical reactions of interest in lithium batteries include salt precipitation and homogeneous electrolyte decomposition. Once the rate of the side reaction is added to the model, it can be used to calculate various possible effects of the side reaction in addition to consumption of current. For example, one could calculate the change in porosity due to precipitation of products of the side reaction[19]. Precipitation of solid species might also affect the surface area of active material available for reaction[50].

A redox shuttle is an example of a desirable side reaction that prevents overcharge. In this situation, a dissolved species R is selected that can be oxidized to species O at some potential close to the maximum desired potential of the cell. O can diffuse away from the positive electrode to be reduced again at the negative electrode, creating an internal short circuit. One might model a redox shuttle by assuming that initially the shuttle is in its reduced form and that the overpotential for reduction of O is very high at the negative electrode, so that the concentration of O is zero at the negative electrode. Narayanan *et al.*[72] give an analysis of the effect of potential on redox shuttle current for the case of nonporous electrodes in which the only current is the shuttle current, the diffusivities of the oxidized and reduced species are equal, and migration is neglected.

Side reactions can introduce error into the measurement of physical properties in three ways[73]. Current is consumed by the side reaction, introducing error into calculations of the amount of current that went into the main reaction. Bulk concentrations of salt or solvent may change if the side reaction is substantial, and soluble products of reaction may affect the

activity of the electrolyte. Finally, the side reaction causes the potential of the electrode to be a mixed (corrosion) potential. The last effect is the most important for measurements of transference numbers using symmetric lithium | lithium cells. It is commonly assumed that the lithium electrode is covered and protected by the SEI layer. However, there is strong evidence that, in many situations, the protection is not complete and side reactions involving the solvent or anion continuously occur. If a concentration gradient exists across the cell, then the mixed potential at the working and counter lithium electrodes will not be the same. The error introduced by the corrosion potential is most significant on concentration-cell measurements at low salt concentrations. Simulations of the type described in this section can be used to analyze how much error is introduced by the side reaction[73]. It may be preferable to use a less reactive reference electrode, such as $Li_4Ti_5O_{12}$[74], to reduce this error.

Several works have explored the effects of side reactions in other battery systems in great detail, and their methodologies are applicable to lithium batteries[59, 75, 76, 77, 8].

4.8 Volume changes and velocity in the electrolyte

Where volume changes and/or solvent velocity are of issue, two equations are needed in addition to the mass balance on the electrolyte. The first is a material balance on the solvent:

$$c_o\left(\frac{\partial \epsilon}{\partial t} + \nabla \cdot \mathrm{v}_o\right) = -\epsilon\frac{\partial c_o}{\partial t} - \mathrm{v}_o \cdot \nabla c_o + a j_o \tag{64}$$

The second relates the change in porosity due to volume change in the i solid phases by j electrochemical reactions occuring at rate $i_{n,j}$ and by k chemical reactions occuring at rate r_k:

$$\frac{\partial \epsilon}{\partial t} = \sum_{solid phases}\left(\sum_l \frac{s_{i,l}\overline{V}_i}{nF} a i_{n.l} - \sum_k s_{i,k}\overline{V}_i r_k\right) \tag{65}$$

Changes in porosity cause changes in the velocity of the solvent by pushing the electrolyte out of or into the pores. Changes in porosity would also effect effective properties such as conductivity (see below). For example, a large electrode volume expansion may increase the effective electronic conductivity while decreasing the effective ionic conductivity, resulting in increased reaction closer to the separator at the expense of reaction within the electrode[78]. Such considerations are generally negligible with insertion electrodes, which achieve high reversibility and thus long cycle life by the very virtue of involving minimal displacement of the active material. However, volume change is of considerable importance in alloy electrodes and systems such as the lithium thionyl-chloride primary battery. In such cases, a reservoir of electrolyte may be incorporated into the battery design to accomodate volume change. Pollard and coworkers[19, 8] include an electrolyte reservoir in a 1-dimensional model by

treating it as a well-mixed region of variable thickness and negligible impact on mass transfer between the separator and positive electrode. While a reservoir of variable volume is an effective method for treating changes in electrolyte volume, it is an approximation to the true behavior of an electrolyte reservoir, which usually sits on top of the electrodes. Improvements to modeling the effect of the electrolyte reservoir on the distribution of electrolyte concentration within the electrodes require a two-dimensional model[79, 80].

Equations 64 and 65 assume that all change in electrode volume is compensated by change in electrolyte volume fraction. This assumption neglects any effects of mechanical stress on changes in electrode area and/or thickness, and may be a poor assumption for alloy or phase-change electrodes[81]. Calculation of such changes in electrode volume would require knowledge of the mechanical properties of the battery container.

4.9 Effective properties in porous media

The values of κ, D, and σ used in equations 3, 12, and 4, respectively, are reduced within the porous electrode relative to their bulk values due to the tortuous path which the ions in solution must make around the solid particles or which the electrons must make around the electrolyte-filled pores. Generally, the effect of volume fraction ϵ_P and tortuousity of the phase of interest on property P in that phase is accounted for by the Bruggeman relation[82], $P = \epsilon_P P_\infty/\tau$, where τ is the tortuosity and is usually related to the porosity by $\tau = \epsilon^{-0.5}$. Because the flux N is defined with respect to superficial area as opposed to electrolyte area, D already gets multiplied once by ϵ in the mass balance, so $D = D_\infty \epsilon^{0.5}$.

In gel electrolytes, in which a liquid electrolyte is imbibed into a polymer matrix, calculation of the effective diffusivity and ionic conductivity based on the apparent volume fraction of electrolyte in the polymer may be complicated by solvation of the polymer by the solvent, increased tortuousity presented by the polymer, and possible interactions of the ions with solvating groups on the polymer. One way to handle these effects empirically is to treat the tortuosity as an adjustable parameter which is fit to measurements of diffusivity in actual gels[35]. This empirical tortuosity parameter appears to depends on the nature of the gel's environment, such as whether the gel is mixed into a porous electrode or free-standing[70]. Such effects may be due to preferential adsorption of the polymer to the solid surface.

Tortuosity also plays a large role in the effective transport properties of polymer electrolytes because obstruction of the sequential motion of polymer chains can block mechanisms of ion transport[83] and because adsorption of the polymer to particles of active material or conductive filler may cause the formation of nanometer-thick glassy polymer films around the solid particles[84]. A better understanding of the effects of tortuosity, polymer-electrode surface forces, and polymer chain length on transport in polymer and gel electrolytes is needed for more accurate treatment of effective transport properties in these systems.

Interparticle contact is of critical performance to the behavior of lithium batteries. Most lithium-ion electrodes contain 2 to 15 wt% conductive filler, such as carbon black, in order to

maintain contact among all the particles of active material and in order to reduce ohmic losses in the electrodes. Presently, there are few models available for predicting contact resistance, and the effect of the weight fraction of conductive filler on the overall electronic conductivity of the composite electrode must be determined experimentally. Doyle *et al.*[35] demonstrate how the full-cell-sandwich model can be used to determine what minimum value of effective electronic conductivity is needed to make solid-phase ohmic resistance negligible. Then, one need only measure the effective conductivity of the composite electrode as a function of filler content, and one need not run separate experiments on complete cells to determine the optimum filler content. Modeling techniques for predicting effective electronic conductivities of composite electrodes are under development, and hold promise to aid in optimizing filler shape and volume fraction[85].

4.10 Use of mass-transfer coefficients

Porous electrode theory treats the inherently random geometries of porous electrodes by using quantities appropriately averaged over the randomly-shaped pore volume, solid volume, pore-wall area, or electrode cross-sectional area[1, 18]. The kinetic equation 19 involves the potential of the solid at the solid-electrolyte boundary, the potential of the electrolyte (which is a function of electrolyte concentration) at the electrolyte-solid boundary, and the exchange-current density evaluated at the electrolyte concentration at the electrolyte-solid boundary. However, the equations presented in this review treat only the average potential and electrolyte concentration at a given position (radial variations in solid concentration are calculated either by the superposition integral or by using a pseudo 2-dimensional geometry, see section 4.1). Thus, the averaging inherent to porous electrode theory introduces some (usually very small) degree of error. Mass-transfer coefficients can be introduced to try to compensate, such as by using an effective mass transfer equation, $j_n = -k_m(c - c_{wall})$, to solve for the concentration at the pore wall. Tsaur and Pollard[8] report that mass transfer within pores has a significant effect on cell performance only for species present in small concentrations. Levich[86] and Wang *et al.*[31] review mass-transfer coefficients in detail.

4.11 2- and 3-dimensional effects

A one-dimensional model assumes that gradients in potential are negligible in the two directions parallel to the current collectors. Such an assumption is valid for laboratory-scale cells, which are generally small and/or use thick, highly conducting current collectors. When scaling up a cell to a full-scale battery, one may be interested in how potential varies along the current collector due to ohmic drop, and how this potential drop affects the current distribution within the battery. In large batteries, ohmic drop down the current collectors may be significant enough to affect the current distribution, with a higher current closer to the tabs. A two- or three-dimensional model may be desirable then in order to optimize the

electrical conductivity (*i.e.*, thickness) of the current collector, length of electrodes, shape of the current collector, and position of tabs, with respect to overall cost, weight, or volume of the cell [87, 88, 89, 90, 91]. They can also be used to understand the potential distribution within the cell and how that distribution affects experimental measurements[92]. The model can either solve the full governing equations treating current and flux as vector quantities, or it can couple the full model for behavior perpendicular to electrode to a simplified resistor-network model for effects parallel to the electrodes[90]. Bernardi *et al.*[80] review two- and three-dimensional battery models and present results for a lead-acid cell.

In the spiral-wound geometry (also called a jelly roll), the radius of curvature of the electrodes decreases as the radius of the spiral increases, thereby creating a two-dimensional geometry. Spiral-wound geometries have been treated by Evans and White[93] and Podlaha and Cheh[94]. Podlaha and Cheh describe a methodology to simulate a spiral-wound configuration with a one-dimensional model consisting of multiple cell layers connected by "virtual" current collectors. They compare simulations of a spiral-wound alkaline cell to that of a bobbin cell with equivalent total reactant surface area.

The primary focus of two- and three-dimensional models of lithium batteries has been to determine the temperature distribution across a large cell or battery stack[95, 96]. The temperature profile across a lithium battery stack is of interest because the rate of cell degradation increases with increasing temperature. As the capacity of the hotter cells in a series-connected stack fades, they will become prone to overcharge and overdischarge, situations which can potentially lead to thermal runaway. Chen and Evans[97] analyze the thermal response of a battery stack to a hot spot created by a short circuit in one cell.

The Biot number is defined as $\mathrm{Bi} = hL/k$, where h is the heat-transfer coefficient with the surroundings, L is a characteristic length of the battery, and k is the effective thermal conductivity. If the Biot number is greater than 0.1, then temperature gradients in the battery cannot be neglected. Newman and Tiedemann[98] discuss how thermal aspect ratios (L^2/k) affect the maximum stack temperature for the case of uniform heat generation. Baker and Verbrugge[89] analyze how nonuniformity in the secondary current distribution, caused by ohmic losses along the current collector, can lead to nonuniformity in the temperature profile of a large cell. They assume constant physical properties and linear kinetics. The analysis uses the perturbation technique to extend the one-dimensional secondary current distribution for porous electrodes derived by Euler and Nonnenmacher[99, 100] to two dimensions, assuming that all current in the porous electrodes and electrolyte flows perpendicular to the current collectors, and all current in the current collectors flows parallel to the curent collectors. A series solution for the temperature profile in the direction parallel to the current collectors is then derived. They find that their parameter $\widetilde{L}$, which depends on the electrical conductivity of the electrodes and current collectors, κ, ϵ, thicknesses of the cell and current collectors, i_0, and cell height (see their Table II and equation 21), determines the importance of considering two-dimensional variations in the secondary current distribution. For $\widetilde{L} \ll 1$, two-dimensional effects can be neglected.

As discussed in section 3.7, transport and kinetic properties generally exhibit an Arrhenius dependence on temperature, leading to a lower rate of heat generation at higher temperatures. Accurate thermal modeling therefore requires coupling of the electrochemical model to the thermal model through the temperature dependence of the physical properties. Several different techniques for such coupling have been presented. Song and Evans[101] solve the coupled equations directly, and present results for a lithium polymer bipolar stack under different thermal management conditions. Pals and Newman present two methods for simplifying the computational time. In the first method, an effective heat-transfer coefficient is computed as a function of cell position in a bipolar stack[28]. In the second, an isothermal model for a single cell is used to compute the heat generation of a cell presently at that temperature within a stack[102]. This method introduces some error regarding the effect of the thermal history of a cell. Verbrugge[103] presents a method for reducing the computational power required to simulate the two- or three-dimensional current and temperature distribution (for the case of constant concentration and linear kinetics) for a battery stack composed of many cells. All of these papers show that the improved transport and kinetics at higher temperature lead to a more uniform stack temperature compared to simulations with constant properties.

5 Analytic Solutions for Special Cases

Solutions to simplified forms of the governing equations can prove useful for several reasons. An analytic solution provides a closed-form relationship between independent and dependent variables, which allows calculation of kinetic and transport properties from experiments designed to meet the requirements of the limiting case. They provide dimensionless terms and closed-form relationships that make it easier to identify the effects of different variables and to identify which forces are dominating behavior. Finally, analytic solutions provide a useful starting point for optimization. Many analytic solutions are for "steady-state" operation. Strictly speaking, there is no steady state in the operation of lithium-ion batteries, because the lithium concentration in the active material is continually changing, thereby changing the potential of the active material. The assumption of steady state allows one to examine effects of other parameters in the absence of change in the active material.

An analytic solution for the steady-state current and potential distributions in a porous electrode neglecting any concentration variations was determined early in the development of porous electrode theory[100]. The ratio of ohmic resistance to kinetic resistance determines the uniformity of the secondary current distribution across the porous electrode. For Tafel kinetics, this ratio is $\delta = \frac{\alpha F I L}{RT}\left(\frac{1}{\kappa}+\frac{1}{\sigma}\right)$, and for linear kinetics it is $\nu^2 = (\alpha_a + \alpha_c)\frac{F a i_0 L^2}{RT}\left(\frac{1}{\kappa}+\frac{1}{\sigma}\right)$[1]. If either of these dimensionless numbers is large, then ohmic resistance dominates kinetic resistance, and the reaction rate will be higher at the separator-electrode interface than in the middle of the porous electrode. L/ν (or L/δ for high currents) is a measure of the

penetration depth of the electrode, *i.e.*, how far the reaction penetrates the electrode before concentration gradients in the electrode and electrolyte drive the reaction further. Increasing the thickness of the electrode beyond the penetration depth has little effect on the reaction-rate distribution and thus the overpotential across the electrode. For pure concentration resistance, neglecting all ohmic and kinetic resistance, the penetration depth is L/γ, where $\gamma_i = \frac{s_i I L}{nF\epsilon D_i c_{i,\infty}}$[1].

The combination of ohmic resistance in the solid and solution phases (neglecting all concentration and kinetic resistance) with transient consumption of active material forms the basis of the reaction-zone model[104, 105], which predicts that the reaction-rate distribution will move as a front across the porous electrode, consuming the active material at the separator-electrode interface first, when the electronic conductivity of the solid phase is much higher than the ionic conductivity of the electrolyte phase. Doyle and Newman[106] expanded the reaction-zone model to the case where potential in the active material varies linearly with state of charge. Atlung *et al.*[107] treated and verified experimentally[108] a similar problem but for ionic and electronic conductivities of equal magnitudes. The reaction-zone model is particularly relevant to studying current distributions and maximum attainable utilization in batteries with ionomer and molten salt electrolytes, in which concentration gradients have a zero or small effect on cell behavior. Full simulations including kinetics and concentration variations showed results similar to the reaction-zone model for cells with molten salt electrolytes[78, 19]. The reaction-zone model is less appropriate for electrolytes with lower diffusion coefficients.

Doyle and Newman[109] present the limiting current for the case of uniform current density in a porous electrode.[3] The limiting current across the separator (assumed to have a porosity of 1.0) and porous electrode depends on the porosity ϵ, separator thickness L_s, and ratio of the thickness of the electrode to that of the separator $r = L_+/L_s$, as given by

$$I_{lim} = \frac{FDc_o}{(1-t_+^o)L_s f(r,\epsilon)} \tag{66}$$

where

$$f(r,\epsilon) = \frac{1}{2(1+\epsilon r)} + \frac{(1+r)^2}{2r\epsilon^{3/2}}$$

$$+\frac{1}{r\epsilon^{3/2}(1+\epsilon r)}\left[\frac{\epsilon}{3} + \frac{\epsilon r}{2} - r - \frac{1}{2} - \frac{\epsilon(1+r)^3}{3}\right] \tag{67}$$

[3]There has been a misunderstanding in the literature[3] as to how this solution was obtained. Recall that when solving the steady-state form of a transient problem, the initial condition enters in as a constraint that the total mass of electrolyte is constant. Eq. 20 of Doyle and Newman's paper contains a typographical error; the second term on the right side should be positive, not negative. In addition, the time constant for solution depletion with a current spike given in eq. 42 is not the time constant used in equations 56 and 57. These equations use the time constant derived when the delta-function reaction rate is left in the differential equation[110], as opposed to being treated as a boundary condition as presented in their Appendix B.

In addition, the authors compare times for the concentration to become depleted for the case of solution diffusion with uniform current, solution diffusion with a current spike at the separator, and solid diffusion at short and long times. Their figure 8, which plots ratios of these limiting times, allows a qualitative estimate of whether solution-phase diffusion, solid-phase diffusion, or ohmic drop dominates capacity limitations, depending upon the physical parameters of the system. Atlung *et al.*[111] describe the concentration gradients in the solid for the limiting case of uniform current density at short and long times.

Darling and Newman[112] provide an analytic solution, using Laplace transforms, to the linearized problem at short times after current is turned on, in order to examine the spike in current that forms at the separator-electrode interface when the exchange current density is very large.

Table 2 lists time constants for various physical phenomena that occur in batteries. Perhaps the most important time constant for design of a battery is the characteristic time of discharge, $q_{electrode}/I$, where I is the applied current and $q_{electrode}$ is the coulombic capacity of the electrode as calculated from the volume fraction of active material, electrode thickness, cell area, and specific coulombic capacity of the active material. Ratios of time constants reveal the relative time scales of physical phenomena. For example, if the the ratio of diffusion time in a solid particle to discharge time is $\ll 1$, then solid diffusion limitations are negligible in that electrode. For a given electrode, the particle size at which solid diffusion will become limiting is that at which this ratio approaches 1[11]. If the ratio of diffusion time in the electrolyte to discharge time is $\ll 1$, then a pseudo-steady-state concentration profile is established in the electrolyte early in the discharge process.

6 Applications for models

6.1 Understanding limiting factors

One of the most useful aspects of computer simulations is that they allow us to ask "What if?": What if we could make the separator infinitely thin, would that remove problems from concentration polarization? What if we increased the transference number at the expense of conductivity, would we gain increased performance? These questions are particularly relevant for the development of polymer electrolytes. Since the three transport properties for a binary electrolyte, κ, D, and t_+^o, all vary substantially with temperature and concentration, and all of these properties are affected by the nature of the polymer and salt, determining which polymer would yield the best performance would require a large number of experiments and would be difficult to analyze. However, simulations can be run easily to compare performance of different polymers in order to evaluate tradeoffs among the transport properties, such as the tradeoff between transference number and conductivity[113] as shown in figure 4. Thomas *et al.*[114] show that most of the concentration depletion in polymer electrolytes occurs inside the porous electrode, rather than in the separator, and discuss the limit of gains that can

be achieved through thinner separators alone. Figure 5 shows the simulated electrolyte concentration for a Li | polymer electrolyte | V_6O_{13} cell during a C/3-rate discharge, for polymers of two sets of transport properties: those that meet USABC goals ("ideal") and those with the properties of the best polymer available today at 40°C.

Doyle *et al.*[2] examine the tradeoffs involved with using a higher salt concentration in polymer electrolytes. Conductivity in polymer electrolytes generally displays a maximum at about 1 to 1.5 M salt concentration. One might then choose to use a salt concentration which yields this maximum conductivity. However, because concentration gradients form upon passage of current, in some operating regimes lower overall resistance might be achieved by using a higher salt concentration. The somewhat lower conductivity in the separator may be more than compensated by the higher conductivity in the porous electrode.

Doyle *et al.*[35] show how the full cell-sandwich model can be used to determine maximum and minimum salt concentrations in the cell as a function of time, position, and current density, in order to evaluate the risk of salt precipitation and the effect of salt depletion on accessible capacity. Experiments verified the model's prediction that salt depletion would limit accessible capacity upon high discharge rates in Bellcore-style plastic lithium batteries. Figure 6 compares model predictions to experimental discharge curves at currents ranging from the C/5 to 7C rate for a Bellcore cell. Figure 7 shows profiles of electrolyte concentration at different times during one of these discharges, at the 3C rate (6.25 mA/cm^2). The time at which the potential drops steeply during discharge corresponds to depletion of salt in the cathode. Most of the concentration polarization is in the porous electrodes, not in the separator. The simulations indicated that increasing the electrolyte volume fraction within the electrodes would reduce concentration polarization and ohmic drop more than would reducing the separator thickness, and this was confirmed by experiments. Ref. [11] evaluates how increasing the salt concentration can increase the accessible capacity by delaying the time at which concentration is driven to zero, and describes how the model can be used to evaluate the maximum concentration that can be used at a given current density before salt precipitation becomes a concern.

While most modeling studies concern themselves with the behavior of the system during passage of current, the relaxation of the system after current is interrupted is of interest for measurement of diffusion coefficients and for determination of cell response to sequential charge-discharge cycles. The governing equations remain unchanged. Fuller *et al.*[115] examine the relaxation of a nonuniform solid concentration, created during passage of current with a nonuniform current distribution. Current flows within the electrode (but with no net current out of the electrode) because of the driving force of the nonuniform state of charge and, to a lesser extent, because of the concentration gradients in the electrolyte. If the open-circuit potential varies steeply with state of charge, then the electrode will rapidly tend towards a uniform concentration. However, if the open-circuit potential varies little with concentration, then there is little driving force for electrochemical equalization in the solid phase. The extreme case of relaxation in a phase-change electrode, in which the open-

circuit potential is constant with state of charge, results in little change in the nonuniform distribution of utilization upon relaxation[116]. Fuller *et al.* show how the presence of a nonuniform solid concentration is actually beneficial when the current is reversed, because reactants are piled up closer to the reacting region (separator-electrode boundary).

Relaxation phenomena affect the accuracy of the "signature-curve" method for obtaining capacity *vs.* discharge rate in a minimum amount of time[117]. In the signature-curve method, an initially fully charged cell is first discharged to a cutoff voltage at the highest rate, C_1, and the capacity it achieves at that rate is recorded. To determine the capacity at the next highest rate, C_2, rather than recharging the cell and then discharging it again at the C_2 rate, the cell is allowed to relax after the end of the previous C_1 discharge, and then discharged at the C_2 rate to the same cutoff voltage. The capacity recorded at the rate C_n is the sum of the capacities achieved in this manner for rates C_1 through C_n. This method saves the time of performing separate discharges and charges at each rate. Ideally, the rest time prior to the next discharge at the C_{n+1} rate is just long enough to allow the cell to relax to the conditions which would have existed if one had discharged the cell at the C_{n+1} rate from full charge to the state of charge reached at the end of the previous C_n-rate discharge. This time is somewhat less than the characteristic time for relaxation of gradients in the state of charge across the electrode, given by $\tau = \frac{nF\overline{V}_{active}L^2\epsilon}{\kappa(dU/d\Theta)}$.

6.2 Optimizing geometric parameters

There are several geometric parameters that can be controlled in the manufacturing and design processes: volume fractions of each phase, especially the electrolyte volume fraction; solid particle diameter; thickness of the electrodes; and separator area, which determines the current density for a given overall applied current. In addition, the initial salt concentration in the electrolyte and the positive-to-negative capacity ratio are design parameters. Modeling can greatly reduce the amount of experiments needed to optimize these parameters. A full-cell simulation model can be coupled to an optimization algorithm to determine the values of the geometric parameters that yield some optimum objective. The objective must be clearly defined by the designer, and could be maximum energy density or maximum average power density for a given discharge time, maximum peak power density at a specified depth of discharge, or some tradeoff between power and energy, such as the "knee" in a Ragone plot[87]. The optimization procedure tells one the optimum geometric parameters which maximize the performance of materials with given thermodynamic, kinetic, and transport properties. One can then use this information on maximum theoretical performance to compare different materials and to evaluate goals.

Optimizations of lithium-polymer batteries for electric vehicles[114] and lithium-ion batteries for hybrid vehicles[118, 11] have been presented. Chiang and Hellweg[119] optimize not just the porosity of the electrode, but how the porosity should vary across an electrode, for maximum power and energy density. The porosity should be higher closer to the separator,

where the highest rate of reaction occurs. Newman[105] presents an optimization methodology to achieve maximum energy density for the case of a battery in which the assumptions of facile kinetics, constant concentration, negligible ohmic drop in the electrode phase, and constant open-circuit potential apply. A lithium battery using an ionomer electrolyte might fall under this category. In this case, the optimal values of geometric parameters such as electrode thickness, area, and porosity depend on the dimensionless parameter $T = U\kappa t_d/qL_s^2$, where t_d is the design time of discharge and q is the coulombic capacity of the electrode per unit volume.

Of particular interest in the design of lithium-ion batteries is the optimization of the positive-to-negative capacity ratio[4]. The issue of balancing capacity is of acute importance in nonaqueous batteries because of the absence of a benign overcharge reaction such as the hydrogen and oxygen evolution reactions which occur in aqueous systems. In the absence of side reactions, one would make the capacities of the positive and negative electrodes nearly equal, with the electrode which behaves more favorably at the end of charge and discharge being limiting. However, in the presence of side reactions, particularly the formation reaction to form the SEI layer on the carbon electrode, determining the optimum balance can be more difficult. One must balance the penalties of having excess mass in either electrode against the risks associated with overcharging or overdischarging particular electrodes[120]. Given experimental data for how much cyclable lithium is consumed by a given side reaction, *e.g.,* SEI formation, models can help one assess the likelihood of risks such as lithium deposition when the negative electrode is undersized or undesirable phase transitions or solvent oxidation when the positive electrode is undersized, in order to find the balance of electrode capacity that maximizes energy density without comprimising safety or cycle life.

6.3 Interpreting experimental data

6.3.1 Measuring transport properties

As mentioned earlier, electrolytes used in lithium batteries are usually concentrated, binary electrolytes that exhibit nonideal behavior. In addition, polymer and gel electrolytes are opaque, highly resistive, and sticky, and therefore their transference numbers are not easily measurable using traditional techniques such as the Hittorf or moving boundary methods. Recent theoretical studies have described the substantial error involved in measuring transference numbers with techniques that assume ideal behavior[14, 15], and have described how experimental data can be interpreted rigorously using concentrated-solution theory to obtain transference numbers. One method is the galvanostatic polarization technique[121, 122, 123]:

$$(1 - t_+^o) = \frac{mc_\infty F(\pi D)^{1/2}}{4} \frac{d\ln c}{dU} \tag{68}$$

where m is the slope of a $\triangle\Phi$ *vs.* $It_i^{1/2}$, where $\triangle\Phi$ is the potential across the electrolyte after galvanostatic polarization at current I for time t_i, and $\frac{dU}{d\ln c}$ is the variation of open-circuit potential with electrolyte concentration.

Pollard and Comte[15] analyzed how to obtain the salt diffusion coefficient and transference number from ac impedance for the case of a binary electrolyte (three species) and for the case of a binary salt in a mixture of two solvents (four species). For the three-species case, the transference number is determined by

$$(1 - t_+^o)/z_-\nu_- = \frac{s_o c}{n c_o} - \frac{s_-}{n\nu_-} - F\sqrt{\frac{Z_w(0)\epsilon A D c}{\nu L c_o \overline{V}_o \left(1 + \frac{d\ln f_\pm}{d\ln c}\right)}} \tag{69}$$

where $Z_w(0)$ is the width of the arc related to transport resistance on a Nyquist plot and the equation allows for the general case in which any of the three species may be involved in reaction at the electrodes. Note that the quantity $t_i^o/z_i\nu_i$ is independent of the choice of speciation in the electrolyte (*e.g.*, degree of dissociation), and it is this quantity which appears in equation 12. Pollard and Comte also present methods to test whether a binary electrolyte obeys the assumptions of dilute solution theory and whether an electrolyte behaves as a three-component or four-component solution.

Darling[30] has discussed how a distribution of particle sizes in a porous electrode can affect the accuracy of measurements of the solid diffusion coefficient using the galvanostatic intermittent titration (GITT)[124], restricted diffusion[125], and ac impedance[126] methods. At short times, as used in GITT, the particles behave like semi-infinite media, and the response is independent of the particle-size distribution. At long times, as used in restricted diffusion and ac impedance, the response is affected by particle size. Therefore, the GITT technique, in cells properly designed to minimize solution-phase diffusion effects (*i.e.*, thin electrodes and use of a reference electrode or thin separator) is preferred for measuring solid diffusivities. Darling uses an analytic solution to the impedance of a porous electrode, neglecting transport in the electrolyte, to derive the following correction to the ac impedance method:

$$D_s = D_{s,app}\frac{\sum_i \epsilon_i R_i^2}{\epsilon_p R_{avg}^2} \tag{70}$$

where ϵ_p is the volume fraction of active material in the electrode, the summation is over all particle sizes and their respective volume fractions in the electrode, D_s is the actual solid diffusion coefficient at a given state of charge, and $D_{s,app}$ is the apparent solid diffusion coefficient one would measure under the assumption that the electrode consisted of uniformly-sized particles of radius R_{avg} with the same volume fraction and surface area as the actual electrode. As described by Ho *et al.*[126], for spherical particles $D_{s,app}$ is extracted from the resistance R_L and capacitance C_L of the electrode extrapolated to zero frequency by the formula

$$D_{s,app} = \frac{R_{avg}^2}{15 R_L C_L} \tag{71}$$

Verbrugge and Koch[46] provide an analytic solution for the potential of a cell during a GITT experiment for the case of a variable diffusion coefficient, given by equations 38 and 39 with a constant binary interaction parameter, and an open-circuit potential which follows a Wohl's expansion for the excess Gibbs free energy. Zhang *et al.* [127] compare model simulations to experiments of cyclic voltammetry on a single particle of lithium manganese oxide spinel.

6.3.2 Correcting open-circuit potential measurements for side reactions

One of the important features of the insertion compounds used in lithium batteries is the complex variation of their thermodynamic potential with lithium concentration. However, the precise relationship between potential and lithium concentration can be obscured when side reactions introduce error into the calculation of lithium concentration from the amount of current passed. Darling and Newman[36] show how a simple spreadsheet model can be used to correct the effects of side reactions on open-circuit-potential measurements. Data from a few slow-scan voltammetric or slow-rate galvanostatic cycles are entered into a spreadsheet with columns of time, current, potential, and apparent lithium concentration, y, as calculated from Faraday's law using the measured current and time. If there are side reactions, curves of potential plotted against apparent y will not return to the same starting value of y after a cycle. The apparent y is then converted to y', the actual lithium concentration corrected for side reactions, by

$$y'(t) = y'(t-1) + (y(t) - y(t-1)) + \triangle y(t) \tag{72}$$

where $\triangle y(t)$ is the amount of lithium reacted by side reactions in the time interval $\triangle t$, which Darling and Newman calculate using the Tafel equation (for an oxidative side reaction)

$$\triangle y(t) = \Psi \triangle t \exp\left(\frac{\alpha_{a,s} F V}{RT}\right) \tag{73}$$

As mentioned in equation 59, Ψ includes both the exchange current density and the open-circuit potential of the side reaction and is given by

$$\Psi = \frac{A L a_s i_{0,s}}{Q} \exp\left(\frac{-\alpha_{a,s} F U_s}{RT}\right) \tag{74}$$

where AL is the volume of the electrode, Q is the capacity in coulombs of the active material in the electrode, and Ψ has units of s^{-1}. One adjusts the value of Ψ and α_s until the charge-discharge curves all begin and end at the same value of y.

6.3.3 ac impedance

Meyers *et al.* [128] present analytic solutions for the impedance of a porous insertion electrode with film resistance, neglecting mass transport in the electrolyte. They present simplified forms of the equation for a single particle and for high-, moderate-, and low-frequency limits, and discuss when solid-phase diffusion overlaps with charge-transfer resistance and also the capacitive effects of the slope of the open-circuit potential. In addition, they demonstrate how to include a distribution of particle sizes in the analytic solution.

When solution-phase mass-transport impedance is also of interest, numerical simulations can be performed. Doyle *et al.*[63] have demonstrated how numerical simulations of ac impedance can be used to understand the contributions of different aspects of a cell to its measured impedance spectrum. With a model, one can simulate different components (separator, electrodes with and without solid, solution, film, charge transfer, and ohmic resistances) separately by making relevant parameters infinite or zero. These different components can then give insight into the impedance of the full cell (see figure 8). For example, they demonstrated how effects due to distributed resistances within a porous electrode and due to the slope of the open-circuit potential could be confused with solid diffusion limitations, and show how ignoring these effects could lead to large errors when calculating solid diffusion coefficients from ac impedance data on porous electrodes.

7 A brief mention of other kinds of modeling

This review has discussed only continuum-scale models. Other types of models are also used in the study of lithium batteries. Emperical models are used to predict battery life by extrapolating experimental results. Statistical mechanical models help in understanding transport on the molecular level and also in understanding thermodynamic properties of insertion compounds. For example, molecular dynamic simulations can be used to understand and predict diffusion in multicomponent solutions, and Monte Carlo simulations can illustrate how polymer motion impacts salt transport in polymer electrolytes. Finally, *ab initio* calculations can be used to predict oxidation and reduction potentials and interaction potentials, in order to understand mechanisms of solvent decomposition, to guide discovery of novel electrode materials, and to provide information on interatomic forces needed for statistical mechanical simulations.

8 List of symbols

a surface area of active material per volume of electrode (m^{-1})
c salt concentration in the electrolyte (mol/m^3 of solution)
c_i concentration of species i (mol/m^3)

c_s concentration of lithium in the solid insertion electrode (mol/m^3)
c_T total concentration of salt and solvent (mol/m^3)
C double-layer capacitance (F/m^2)
C_p heat capacity (J/m^{2}K)
D_i diffusion coefficient of species i in dilute solution theory (m^2/s)
D salt diffusion coefficient (m^2/s)
$\mathcal{D}$ diffusion coefficient based on thermodynamic driving force (m^2/s)
D_s diffusion coefficient of lithium in an insertion electrode (m^2/s)
$\mathcal{D}_{ij}$ diffusion coefficient for interaction of species i and j (m^2/s)
$f_\pm$ mean molar activity coefficient of an electrolyte
F Faraday's constant, 96487 C/equiv
i_n transfer current normal to the surface of the active material (A/m^2)
i_0 exchange current density (A/m^2)
i_2 current density (A/m^2 superficial area) in the electrolyte
I total current density in the cell (A/m^2)
j total flux due to reaction (mol/s·m^2 of active material)
k thermal conductivity (W/m^2·K)
k_a, k_c rate constants for the anodic and cathodic directions of a reaction
k_m mass transfer coefficient (m/s)
L thickness of an electrode (m)
L_+, L_s, L_- thickness of positive electrode, separator, or negative electrode (m)
m molality (mol/kg)
M_i symbol for the chemical formula of species i or molecular weight (g/mol)
n number of electrons involved in a half reaction
N_i flux of species i (mol/s·m^{2}of apparent area)
q charge on the electrode side of the double layer (C/m^2)
q_i surface charge density of species i on the solution side of the double layer (C/m^2)
$\dot{Q}$ heat-generation rate (W/m^2)
r radial position across a spherical particle (m)
r_k rate of chemical reaction k (mol/s·m^3)
R universal gas constant, 8.3143 J/mol·K, or radius of a particle (m)
R_{film} effective resistance of a solid-electrolyte interphase (Ω·cm^2)
s stoichiometric coefficient, positive for anodic products
t time (s)
t_i^o transference number of species i with respect to the solvent velocity
T temperature (K)
u mobility (cm^2·mol/J· s)
U thermodynamic potential measured with respect to a lithium reference electrode (V)
v velocity (m/s)
V cell potential (V)

$\overline{V}$ molar volume (m^3/mol)
x position across cell (m)
y stoichiometry of lithium in an insertion electrode
z_i charge of ion i

Greek
α transfer coefficient
β symmetry factor for an elementary reaction
ϵ volume fraction (of electrolyte unless otherwise specified)
Γ_i excess concentration of species i in the double layer (mol/m^2)
κ effective ionic conductivity (S/m)
μ chemical potential (J/mol)
ν_i moles of ion i produced when a mole of its salt dissociates
ν number of moles of ions into which a mole of electrolyte dissociates
σ effective electronic conductivity of a porous electrode (S/m)
Θ fraction of total lithium insertion sites which are occupied by lithium
Θ_s site on the lattice of the insertion material which can be occupied by lithium
Θ_p site on the lattice of a crystalline polymer which can be occupied by lithium salt
Φ potential
$\gamma_\pm$ mean molal activity coefficient
γ_i exponent for the dependence of i_0 on the concentration of species i

Superscripts
o property is with respect to solvent velocity or initial condition
Θ secondary reference state of the chemical potential

Subscripts
a anodic
c cathodic
dl double layer
e electrolyte
f faradaic
i species i
lim limiting current
m main reaction
n electrochemical flux normal to surface of active material
o solvent in an electrolytic solution
s side reaction
1 electrode phase
2 electrolyte phase

$-$ anion
$+$ cation
∞ bulk property

References

[1] J. Newman and W. Tiedemann, *AIChE J.*, **21**, 25 (1975).

[2] M. Doyle, T. F. Fuller, and J. Newman, *J. Electrochem. Soc.*, **140**, 1526 (1993).

[3] G. G. Botte, V. R. Subramanian, and R. E. White, *Electrochimica Acta*, **45**, 2595 (2000).

[4] P. Arora, R. E. White, and M. Doyle, *J. Electrochem. Soc.*, **145**, 3647 (1998).

[5] D. Wheeler and J. Newman, in *AIChE Annual Meeting*, p. paper 126h, Reno, Nevada, November 4-9 2001.

[6] K. S. Chen, G. H. Evans, R. S. Larson, M. E. Coltrin, and J. Newman, in *Proceedings of the Electrochemical Society*, Boston, MA, November 1998.

[7] W. G. Sunu and D. N. Bennion, *J. Electrochem. Soc.*, **127**, 2007 (1980).

[8] K. C. Tsaur and R. Pollard, *J. Electrochem. Soc.*, **133**, 2296 (1986).

[9] Z. Mao and R. E. White, *J. Power Sources*, **43-44**, 181 (1993).

[10] J. S. Newman, *Electrochemical Systems.* Prentice-Hall Inc., Englewood Cliffs, New Jersey, 2nd ed., 1991.

[11] T. F. Fuller, M. Doyle, and J. Newman, *J. Electrochem. Soc.*, **141**, 1 (1994).

[12] M. Ue and S. Mori

[13] G. E. Blomgren, in *Proceedings of the Electrochemical Society* (E. B. Yeager, B. Schlumm, G. Blomgren, D. R. Blakenship, V. Leger, and J. Akridge, eds.), vol. 80-7, p. 35, 1980.

[14] M. Doyle and J. Newman, *J. Electrochem. Soc.*, **142**, 3465 (1995).

[15] R. Pollard and T. Comte, *J. Electrochem. Soc.*, **136**, 3734 (1989).

[16] R. B. Bird, W. E. Stewart, and E. N. Lightfoot, *Transport Phenomena.* John Wiley and Sons, Inc., New York, 1960.

[17] L. Onsager, *Annals New York Acad. Sciences*, **46**, 241 (1945).

[18] J. S. Dunning, *Analysis of Porous Electrodes with Sparingly Soluble Reactants*. Ph.D. thesis, University of California, Los Angeles, 1971.

[19] R. Pollard and J. Newman, *J. Electrochem. Soc.*, **128**, 491 (1981).

[20] M. W. Verbrugge and B. J. Koch, *J. Electrochem. Soc.*, **143**, 600–608 (1996).

[21] J. Newman, *Ind. Eng. Chem. Res.*, **34**, 3208 (1995).

[22] S. A. Hallaj, H. Maleki, J. S. Hong, and J. R. Selman, *J. Power Sources*, **83**, 1 (1999).

[23] K. Kanari, K. Takano, Y. Saito, and T. Masuda, in *Proceedings of the International Workshop on Advanced Batteries*, Osaka, Japan, February 22-24 1995.

[24] D. Bernardi, E. Pawlikowski, and J. Newman, *J. Electrochem. Soc.*, **132**, 5 (1985).

[25] L. Rao and J. Newman, *J. Electrochem. Soc.*, **144**, 2697 (1997).

[26] K. E. Thomas and J. Newman. to be published.

[27] K. E. Thomas, C. Bogatu, and J. Newman, *J. Electrochem. Soc.*, **148**, A570 (2001).

[28] C. R. Pals and J. Newman, *J. Electrochem. Soc.*, **142**, 3274 (1995).

[29] G. G. Botte, B. A. Johnson, and R. E. White, *J. Electrochem. Soc.*, **146**, 914 (1999).

[30] R. M. Darling, *Lithium Manganese Oxide Spinel Electrodes*. Dissertation, University of California, Berkeley, CA, December, 1998.

[31] C. Y. Wang, W. B. Gu, and B. Y. Liaw, *J. Electrochem. Soc.*, **145**, 3407 (1998).

[32] B. Wu and R. E. White, *J. Power Sources*, **92**, 177 (2001).

[33] Y. Zhang and H. Y. Cheh, *J. Electrochem. Soc.*, **146**, 850 (1999).

[34] M. Doyle and J. Newman, *Electrochimica Acta*, **40**, 2191 (1995).

[35] M. Doyle, J. Newman, A. S. Gozdz, C. N. Schmutz, and J. M. Tarascon, *J. Electrochem. Soc.*, **143**, 1890 (1996).

[36] R. Darling and J. Newman, *J. Electrochem. Soc.*, **145**, 990 (1998).

[37] F. B. Hildebrand, *Advanced Calculus for Applications*. Prentice-Hall Inc., Englewood Cliffs, New Jersey, 2nd ed., 1976.

[38] M. J. Matlosz, *Experimental Methods and Software Tools for the Analysis of Electrochemical Systems.* Ph.D. thesis, University of California, Berkeley, 1985.

[39] C. Wagner, *J. Mathematics and Phyics*, **34**, 289 (1954).

[40] A. Acrivos and P. L. Chambre, *Ind. Eng. Chem.*, **49**, 1025 (1957).

[41] C. M. Doyle, *Design and Simulation of Lithium Rechargeable Batteries.* Dissertation, LBL Report 37650, University of California, Berkeley, CA, August, 1995.

[42] W. McKinnon and R. Haering, "Physical Mechanisms of Intercalation,", in *Modern Aspects of Electrochemistry* (R. White, J. Bockris, and B. Conway, eds.), vol. 15, 235–304, Plenum, New York, 1983.

[43] A. Anani, S. Crouch-Baker, and R. A. Huggins, *J. Electrochem. Soc.*, **134**, 3098 (1987).

[44] R. Darling and J. Newman, *J. Electrochem. Soc.*, **146**, 3765 (1999).

[45] H. Kanoh, Q. Feng, T. Hirotsu, and K. Ooi, *J. Electrochem. Soc.*, **143**, 2610 (1996).

[46] M. W. Verbrugge and B. J. Koch, *J. Electrochem. Soc.*, **146**, 833 (1999).

[47] B. Paxton and J. Newman, *J. Electrochem. Soc.*, **143**, 1287 (1996).

[48] Z. Mao and R. E. White, *J. Electrochem. Soc.*, **141**, 151 (1994).

[49] R. Pollard, *Mathematical Modeling of the Lithium-Aluminum, Iron Sulfide Battery.* Dissertation, LBL Report 10197, University of California, Berkeley, CA, December, 1979.

[50] J. Dunning, D. N. Bennion, and J. Newman, *J. Electrochem. Soc.*, **120**, 906 (1973).

[51] M. Abyanch and M. Fleischmann, in *Proceedings of the Electrochemical Society* (R. E. White, M. W. Verbrugge, and J. F. Stockel, eds.), vol. 91-10, p. 96, Pennington, NJ, 1991.

[52] J. S. Chen and H. Y. Cheh, *J. Electrochem. Soc.*, **140**, 1213 (1993).

[53] D. M. Bernardi, *J. Electrochem. Soc.*, **137**, 1670 (1990).

[54] V. Srinivasan, J. W. Weidner, and R. E. White, *J. Solid State Electrochem.*, **4**, 367 (2000).

[55] M. Sinha, *A Mathematical Model for the Porous Nickel Hydroxide Electrode.* Ph.D. thesis, University of California, Los Angeles, 1982.

[56] M. E. Orazem and J. Newman, *Modern Aspects of Electrochemistry*, vol. 18, ch. Photoelectrochemical Devices for Solar Energy Conversion. Plenum Press, New York, 1986.

[57] M. E. Orazem and J. Newman, *J. Electrochem. Soc.*, **131**, 2569 (1984).

[58] H. S. Carslaw and J. C. Jaeger, *Operational Methods in Applied Mathematics*. Oxford University Press, London, 2nd ed., 1948.

[59] K. P. Ta and J. Newman, *J. Electrochem. Soc.*, **145**, 3860 (1998).

[60] R. Darling and J. Newman, *J. Electrochem. Soc.*, **144**, 4201 (1997).

[61] G. S. Nagarajan, J. W. V. Zee, and R. M. Spotnitz, *J. Electrochem. Soc.*, **145**, 771 (1998).

[62] A. B. Yu, R. P. Zou, and N. Standish, *Ind. Eng. Chem. Res.*, **35**, 3730 (1996).

[63] M. Doyle, J. P. Meyers, and J. Newman, *J. Electrochem. Soc.*, **147**, 99 (2000).

[64] B. Pillay, *Design of Electrochemical Capacitors for Energy Storage*. Ph.D. thesis, University of California, Berkeley, 1996.

[65] I. Ong and J. Newman, *J. Electrochem. Soc.*, **146**, 4360 (1999).

[66] V. Battaglia and J. Newman, *J. Electrochem. Soc.*, **142**, 1423 (1995).

[67] K. J. Vetter, *Electrochemical Kinetics, Theoretical and Experimental Aspects*. Academic Press, New York, 1967.

[68] K. C. Tsaur and R. Pollard, *J. Electrochem. Soc.*, **131**, 975 (1984).

[69] K. C. Tsaur and R. Pollard, *J. Electrochem. Soc.*, **131**, 984 (1984).

[70] P. Arora, M. Doyle, A. S. Gozdz, R. E. White, and J. Newman, *J. Power Sources*, **88**, 219 (2000).

[71] P. Arora, M. Doyle, and R. E. White, *J. Electrochem. Soc.*, **146**, 3543 (1999).

[72] S. R. Narayanan, S. Surampudi, A. I. Attia, and C. P. Bankston, *J. Electrochem. Soc.*, **138**, 2224 (1991).

[73] H. Hafezi and J. Newman. to be published.

[74] A. Blyr, G. Amatucci, D. Guyomard, Y. Chabre, and J. M. Tarascon, *J. Electrochem. Soc.*, **145**, 194 (1999).

[75] Z. Mao and R. E. White, in *Proceedings of the Electrochemical Society* (R. E. White, M. W. Verbrugge, and J. F. Stockel, eds.), vol. 91-10, p. 46, Pennington, NJ, 1991.

[76] E. J. Podlaha and H. Y. Cheh, *J. Electrochem. Soc.*, **141**, 15 (1994).

[77] D. M. Bernardi and M. K. Carpenter, *J. Electrochem. Soc.*, **142**, 2631 (1995).

[78] D. Bernardi and J. Newman, *J. Electrochem. Soc.*, **134**, 1309 (1987).

[79] W. B. Gu, C. Y. Wang, J. W. Weidner, R. G. Jungst, and G. Nagasubramanian, *J. Electrochem. Soc.*, **147**, 427 (2000).

[80] D. Bernardi, H. Gu, and A. Y. Schoene, *J. Electrochem. Soc.*, **140**, 2250 (1993).

[81] D. Bernardi, E. Pawlikowski, and J. Newman, *J. Electrochem. Soc.*, **135**, 2922 (1988).

[82] D. A. G. Bruggeman, *Annalen der Physik*, **24**, 636–679 (1935).

[83] D. R. Shriver, R. Dupon, and M. Stainer, *J. Power Sources*, **9**, 383 (1983).

[84] G. Tsagaropoulos and A. Eisenberg, *Macromolecules*, **28**, 6067 (1995).

[85] X. Cheng, C. Wang, A. M. Sastry, and S. B. Choi, *J. Engineering Materials and Tech.*, **121**, 514 (1999).

[86] V. G. Levich, *Physicochemical Hydrodynamics.* Prentice-Hall, Inc., Englewood Cliffs, NJ, 2 ed., 1962.

[87] G. G. Trost, V. Edwards, and J. S. Newman, *Chemical Reaction and Reactor Engineering*, ch. Electrochemical Reaction Engineering, pp. 923–972. Marcel Dekker, Inc., New York, 1987.

[88] M. W. Verbrugge, *J. Electrostatics*, **34**, 61 (1995).

[89] D. R. Baker and M. W. Verbrugge, *J. Electrochem. Soc.*, **146**, 2413 (1999).

[90] W. H. Tiedemann and J. Newman, in *Proc. Symp. Battery Design and Opt.* (S. Gross, ed.), vol. 79-1, p. 39, The Electrochemical Society, 1979.

[91] W. H. Tiedemann and J. Newman, in *154th Meeting of the Electrochemical Society*, p. 169, 1979.

[92] J. Newman and W. Tiedemann, *J. Electrochem. Soc.*, **140**, 1961 (1993).

[93] T. I. Evans and R. E. White, *J. Electrochem. Soc.*, **136**, 2145 (1989).

[94] E. J. Podlaha and H. Y. Cheh, *J. Electrochem. Soc.*, **141**, 1751 (1994).

[95] J. Lee, K. W. Choi, N. P. Yao, and C. C. Christiansen, *J. Electrochem. Soc.*, **133**, 1286 (1986).

[96] Y. Chen and J. W. Evans, *J. Electrochem. Soc.*, **141**, 2947 (1994).

[97] Y. Chen and J. W. Evans, *J. Electrochem. Soc.*, **143**, 2708 (1996).

[98] J. Newman and W. Tiedemann, *J. Electrochem. Soc.*, **142**, 1054 (1995).

[99] J. Euler and W. Nonnenmacher, *Electrochimica Acta*, **2**, 268 (1960).

[100] J. Newman and C. W. Tobias, *J. Electrochem. Soc.*, **109**, 1183 (1962).

[101] L. Song and J. W. Evans, *J. Electrochem. Soc.*, **147**, 2086 (2000).

[102] C. R. Pals and J. Newman, *J. Electrochem. Soc.*, **142**, 3282 (1995).

[103] M. W. Verbrugge, *AIChE J.*, **41**, 1550 (1995).

[104] W. Tiedemann and J. Newman, *J. Electrochem. Soc.*, **122**, 1482 (1975).

[105] J. Newman, *J. Electrochem. Soc.*, **142**, 97 (1995).

[106] M. Doyle and J. Newman, *J. Power Sources*, **54**, 46 (1995).

[107] S. Atlung, B. Zachau-Christiansen, K. West, and T. Jacobsen, *J. Electrochem. Soc.*, **131**, 1200 (1984).

[108] B. C. Knutz, K. West, B. Zachau-Christiansen, and S. Atlung, *J. Power Sources*, **43-44**, 733 (1993).

[109] M. Doyle and J. Newman, *J. Appl. Electrochem.*, **27**, 846 (1997).

[110] M. Doyle and J. Newman, "Analysis of Capacity-Rate Behavior Using Simplified Models for the Discharge Process of Lithium Batteries,", unpublished, 1997.

[111] S. Atlung, K. West, and T. Jacobsen, *J. Electrochem. Soc.*, **126**, 1311 (1979).

[112] R. Darling and J. Newman, *J. Electrochem. Soc.*, **144**, 3057 (1997).

[113] M. Doyle, T. F. Fuller, and J. Newman, *Electrochimica Acta*, **39**, 2073 (1994).

[114] K. E. Thomas, S. E. Sloop, J. B. Kerr, and J. Newman, *J. Power Sources*, **89**, 132 (2000).

Table 1: Parameters required for the model. Values must be specified for both electrodes. All material properties can be functions of composition and temperature.

thermodynamic	kinetic	transport	geometric
U	i_0	$\mathcal{D}$	a
ρ (of all components)	α_a, α_c	D_s	L_+, L_s, L_-
$c_{s,max}$	R_{film}	t_+^o	R
$f_\pm$		κ	ϵ(of electrolyte, active, and filler)
initial c and c_s		σ	
C_p			
$\partial U/\partial T$			

[115] T. F. Fuller, M. Doyle, and J. Newman, *J. Electrochem. Soc.*, **141**, 982 (1994).

[116] R. Pollard and J. Newman, *J. Electrochem. Soc.*, **128**, 503 (1981).

[117] M. Doyle, J. Newman, and J. Reimers, *J. Power Sources*, **52**, 211 (1994).

[118] C. Fellner and J. Newman, *J. Power Sources*, **85**, 229 (2000).

[119] Y. M. Chiang and B. Hellweg, in *200th meeting of the Electrochemical Society*, p. 144, San Francisco, CA, September 3-7 2001.

[120] D. Guyomard and J. M. Tarascon, *Solid State Ionics*, **69**, 222 (1994).

[121] Y. Ma, M. Doyle, T. F. Fuller, M. M. Doeff, L. C. de Jonghe, and J. Newman, *J. Electrochem. Soc.*, **142**, 1859 (1995).

[122] H. Hafezi and J. Newman, *J. Electrochem. Soc.*, **147**, 3036 (2000).

[123] P. Georen and G. Lindbergh, *Electrochimica Acta*, **47**, 577 (2001).

[124] W. Weppner and R. A. Huggins, *J. Electrochem. Soc.*, **114**, 1569 (1977).

[125] J. Newman and T. W. Chapman, *AIChE J.*, **19**, 343 (1973).

[126] C. Ho, I. D. Raistrick, and R. A. Huggins, *J. Electrochem. Soc.*, **127**, 343 (1980).

[127] D. Zhang, B. N. Popov, and R. E. White, *J. Electrochem. Soc.*, **147**, 831 (2000).

[128] J. P. Meyers, M. Doyle, R. M. Darling, and J. Newman, *J. Electrochem. Soc.*, **147**, 2930 (2000).

[a] ν_s is a measure of the current distribution in a porous electrode under linear kinetics with a film resistance[65]: $\nu_s = aL^2 \left(\frac{1}{\kappa} + \frac{1}{\sigma}\right) / \left(R_{film} + \frac{RT}{Fi_0(\alpha_a+\alpha_c)}\right)$.

Table 2: Time constants of different physical phenomena

Time constant	Phenomena
$q_{electrode}/I$	discharge of an electrode of coulombic capacity $q_{electrode}$
R^2/D_s	diffusion in a spherical particle
L^2/D	diffusion in the electrolyte
$\pi a C L^2 \left(\frac{1}{\kappa}+\frac{1}{\sigma}\right)\left[\frac{\frac{2\kappa\sigma}{\kappa^2+\sigma^2}+\cosh\nu_s}{2\nu_s\sinh\nu_s}\right]^2$	double-layer charging of a porous electrode[a]
$\frac{nF\overline{V}_{active}L^2\epsilon}{\kappa(\partial U/\partial\Theta)}$	relaxation of gradients in utilization across an electrode

Figure 1: Diagram of a lithium-ion cell.

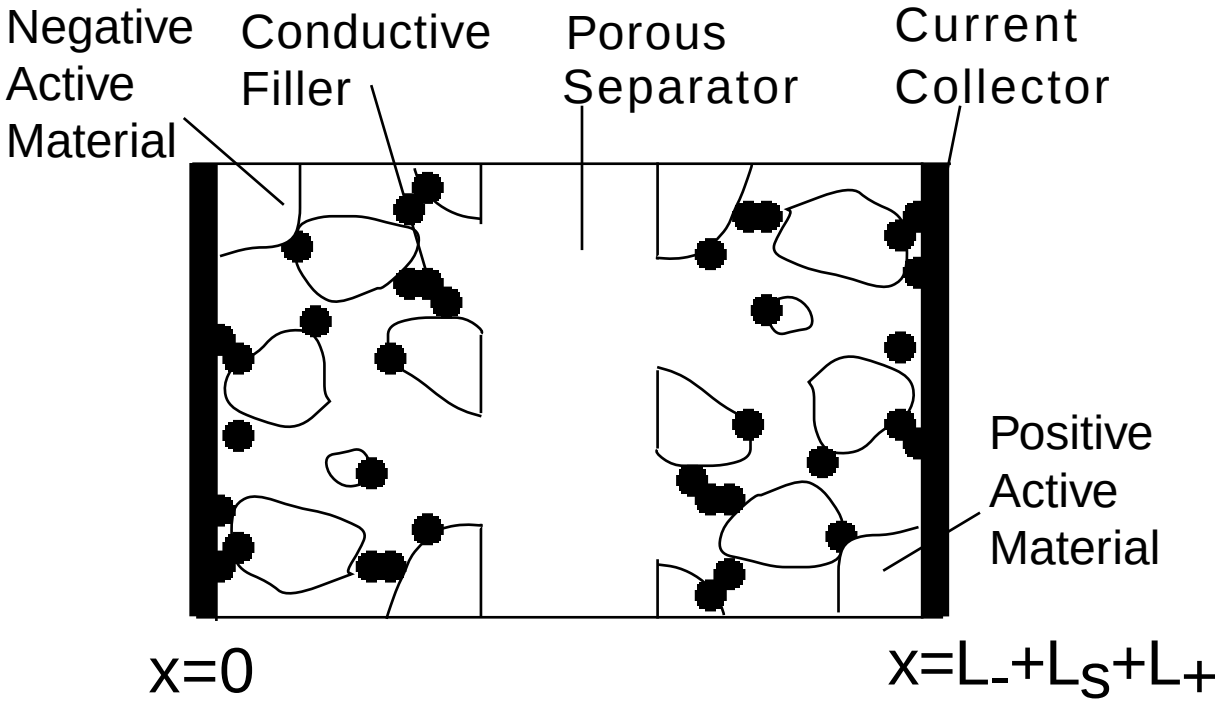

Figure 2: Equilibrium potentials at the surface of particles of two sizes during a charge and discharge. The larger particle has a larger concentration overpotential. From ref. [60].

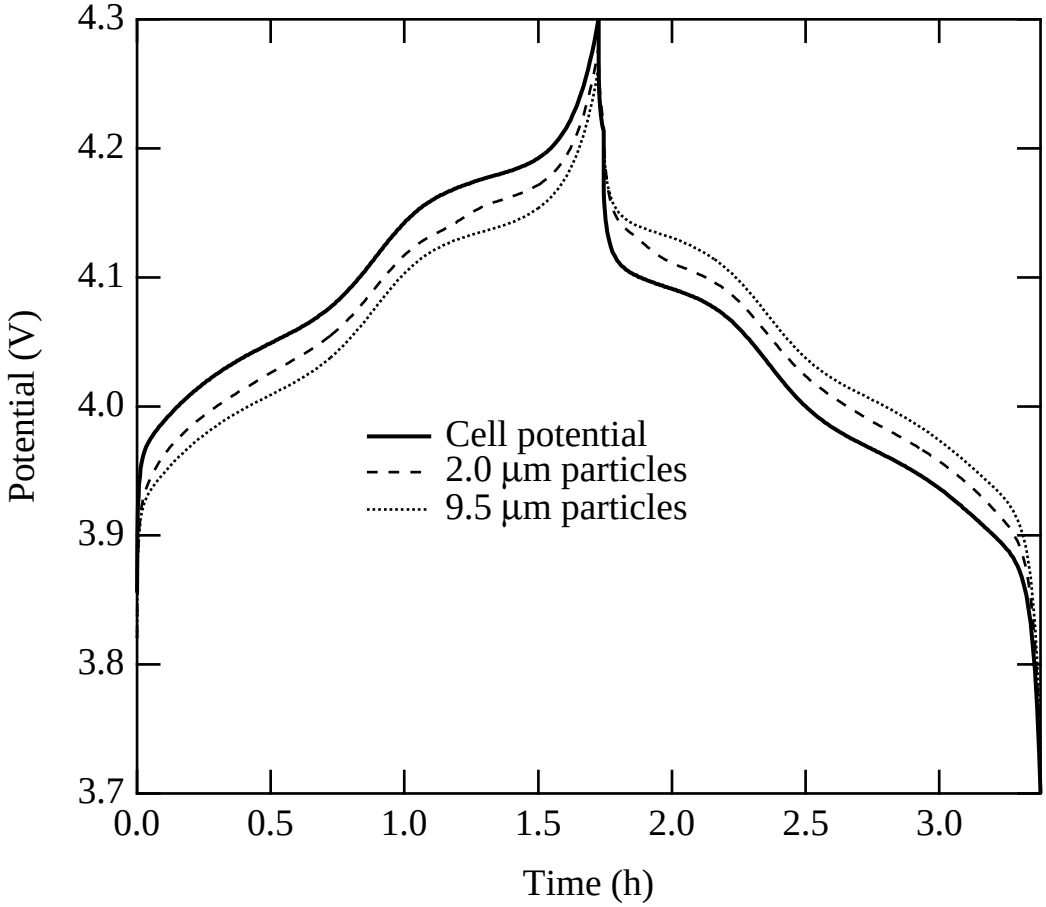

Figure 3: Profiles of $\Phi_1 - \Phi_2$ across a porous petroleum coke electrode at different times during a C/2-rate (-1.146 mA/cm^2) charge. Time since the beginning of charge is indicated in minutes. After 106 minutes, the potential near the separator interface has dropped below the potential for lithium deposition. From ref. [35]

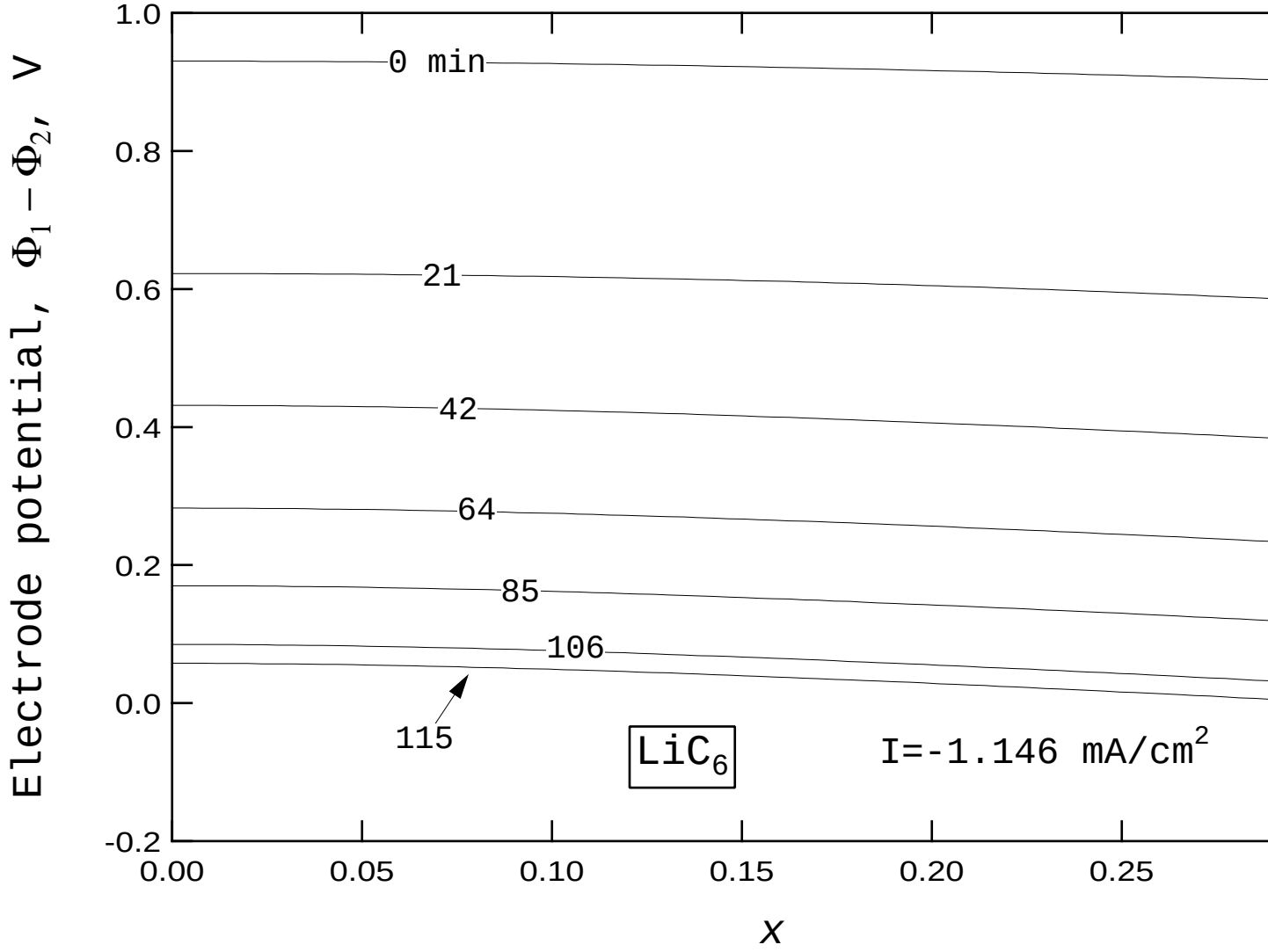

Figure 4: Ragone plot for Li | $LiMn_2O_4$ cells with different electrolytes. Solid lines: ionomer (unity transference number) with conductivity indicated as parameter. Dashed line: polymer electrolyte with $t_+^o = 0.2$, $D = 7.5\times10^{-8}$ cm^2/s, and conductivity of 2 to 3.5×10^{-4} S/cm (depending on electrolyte concentration). For this system, the higher transference number of the ionomer outweighs its lower conductivity when the decrease in conductivity is less than a factor of 10. From ref. [113].

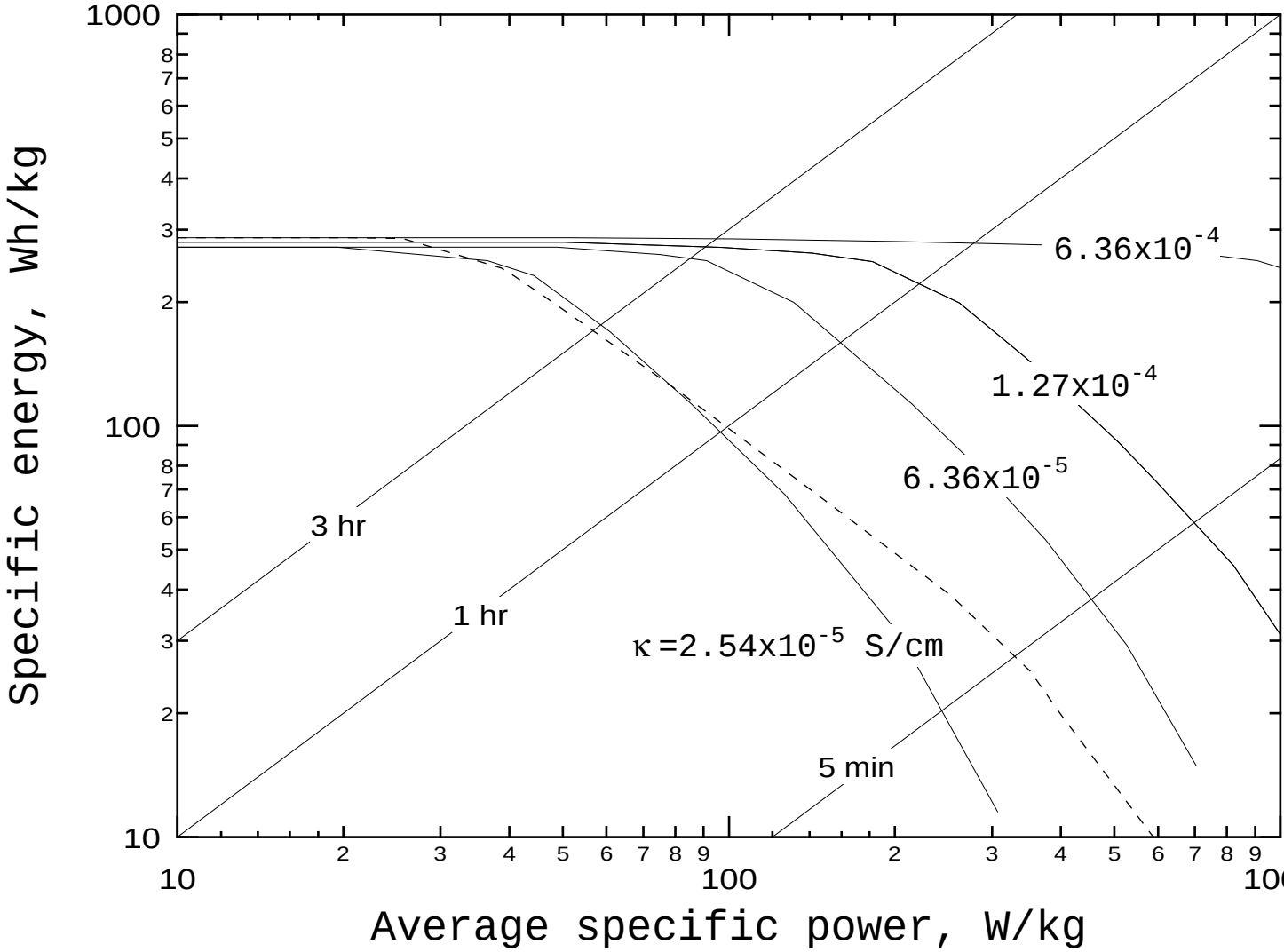

Figure 5: Electrolyte concentration across a Li | polymer | V_6O_{13} cell during C/3-rate discharge for a polymer with $\kappa = 10^{-3}$ S/cm, t_+^o=0.3, and D=10^{-7} cm^2/s ("ideal") and a polymer with $\kappa = 10^{-4}$ S/cm, $t_+^o = 0.1$, and D=6×10^{-9} cm^2/s ("available" at 40°C). The separator is 50 microns thick. The polymer with poorer transport properties develops a large concentration polarization within the positive electrode that severely limits the utilization of the active material. Simply making the separator thinner will not solve this problem. From ref. [114].

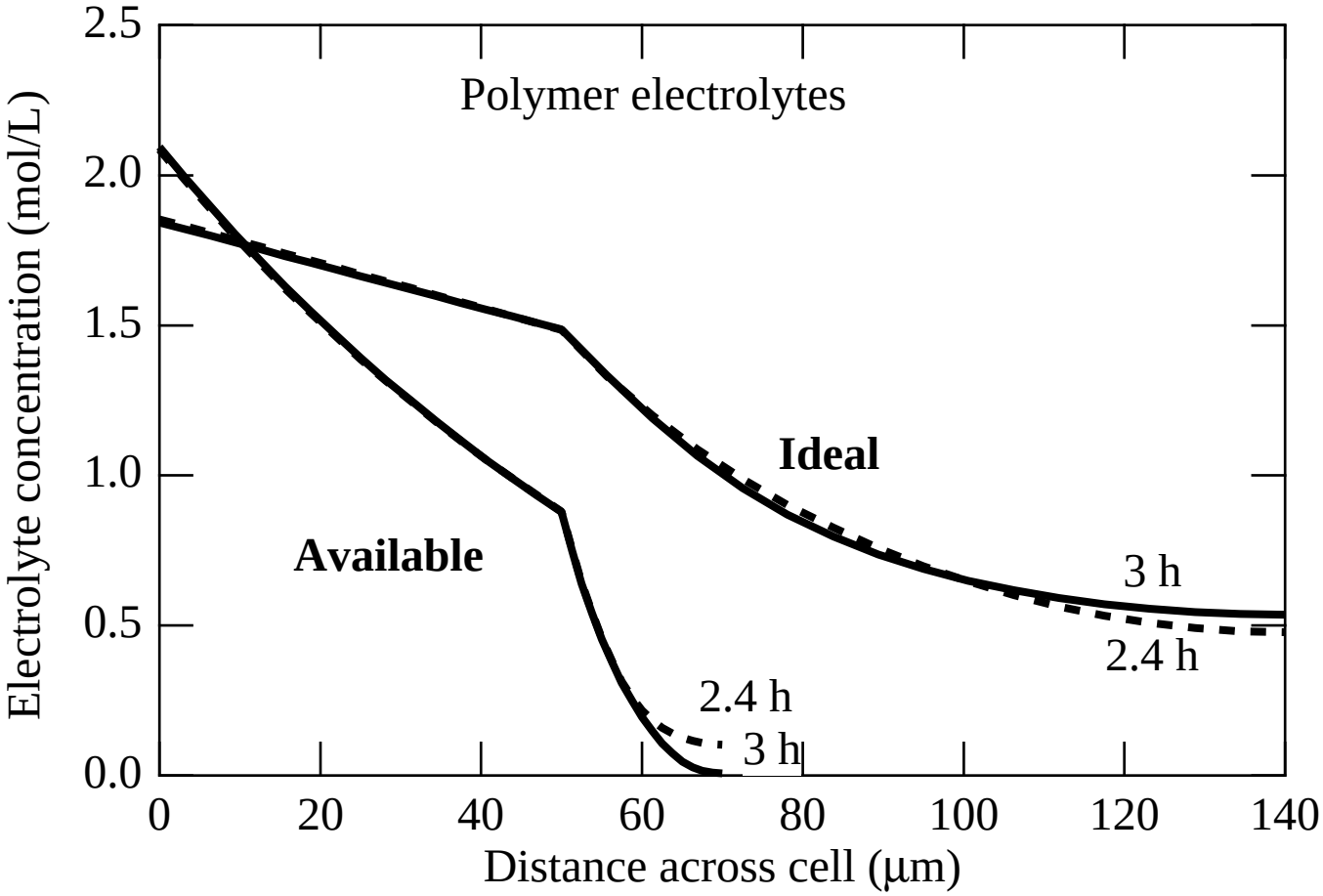

Figure 6: Cell potential during discharge at rates ranging from C/5 (0.4167 mA/cm^2) to 7C (14.56 mA/cm^2) for a Bellcore-style plastic lithium ion cell. Markers: experiment. Lines: simulation. From ref. [35].

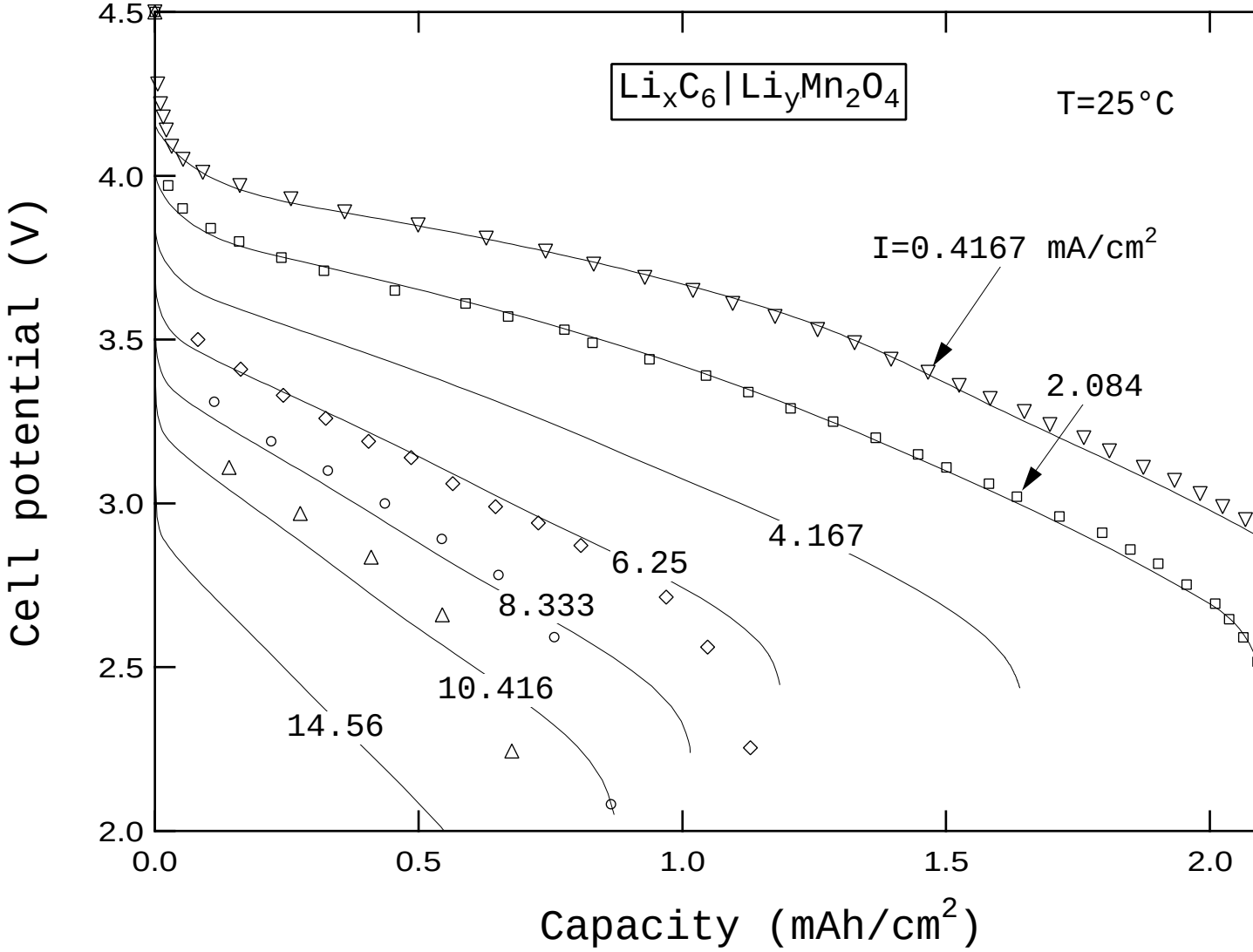

Figure 7: Salt concentration profiles for the same cell as figure 6 during galvanostatic discharge at 6.25 mA/cm^2 (3C rate). The separator region is set off by dashed lines. Time since the beginning of discharge is given in minutes. After eleven minutes into the discharge, the electrolyte is depleted in the cathode. From ref. [35].

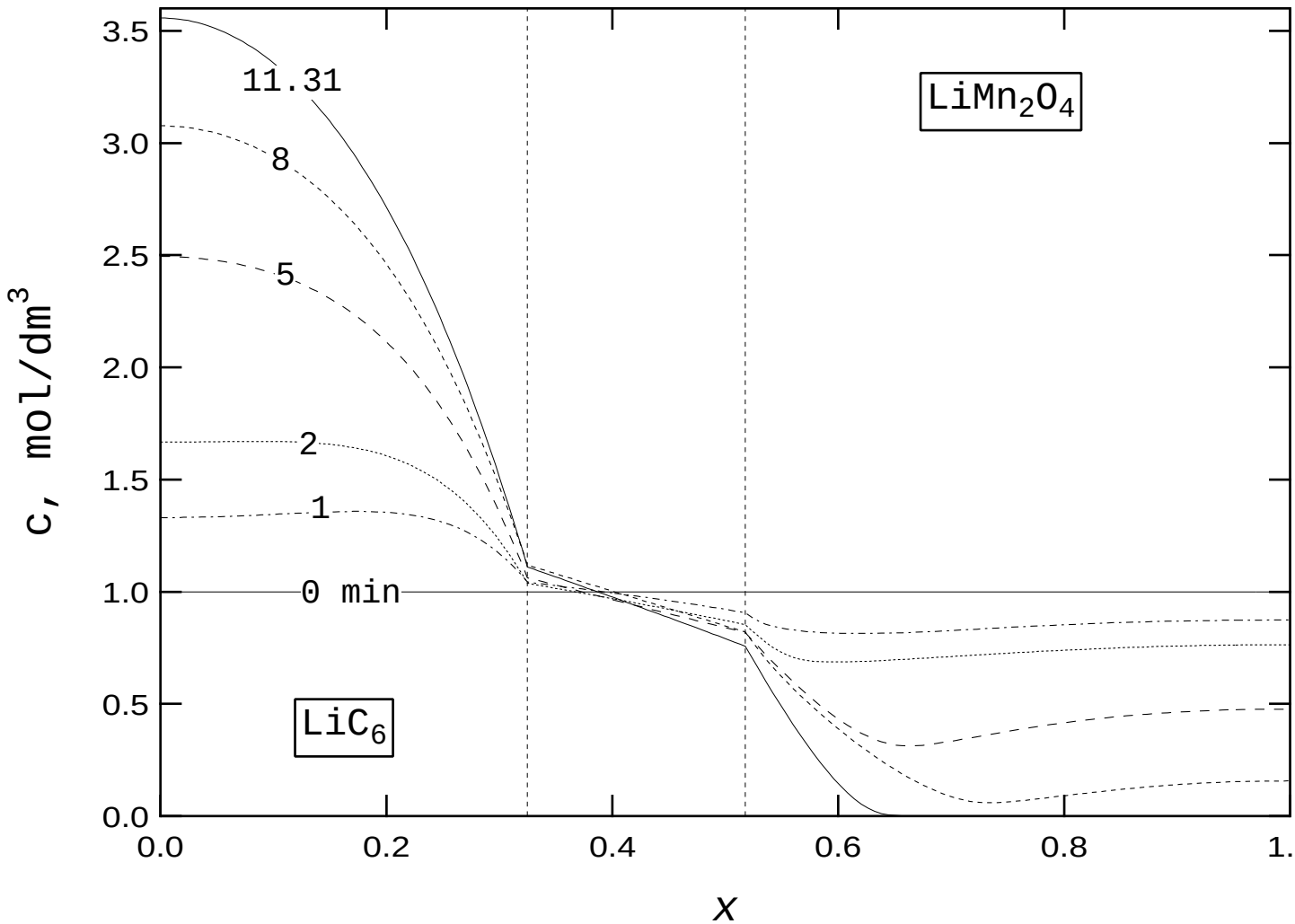
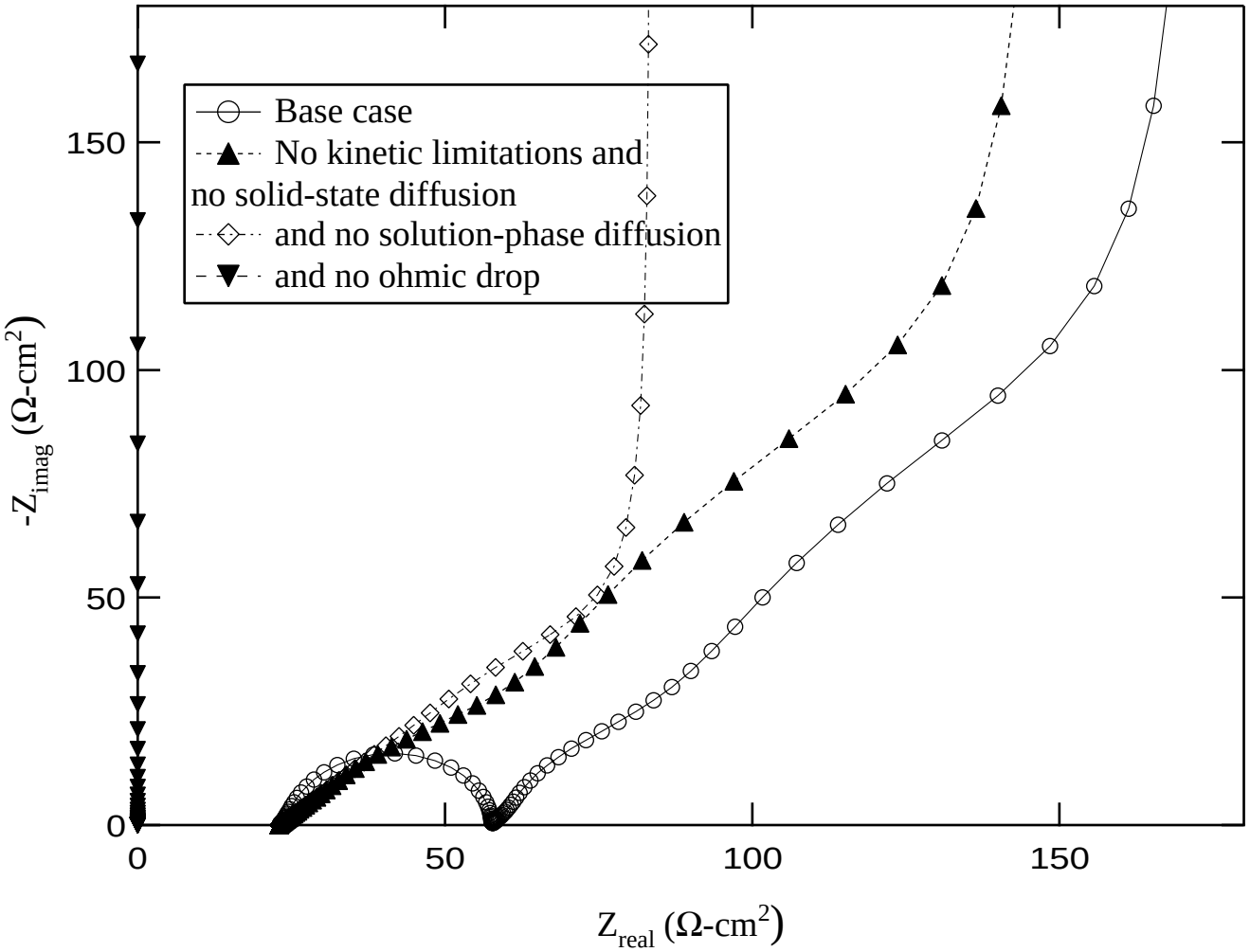
Figure 8: Simulated impedance of a Li | $PEO_{18}LiCF_3SO_3$ | $LiTiS_2$ cell. The base case is the impedance of the full cell. The components of this impedance can be elucidated by progressively setting parameters to have zero impedance. Thus, first we see that the semicircle is due to kinetic impedance and that solid diffusion has little effect, then that solution-phase diffusion within the porous electrode is responsible for much of the shape of the impedance spectrum at low frequencies, and finally that ohmic drop and the capacity of the porous electrode are responsible for a 45° slope at moderate frequencies that shifts to a verticle line at low frequencies. From ref. [63].